Response to editor

please note, that if only one model is concerned, the title of a GMD manuscript should state the model name (or its acronym) and a version number. These are also important to know in the case of an evaluation, as different versions might perform differently for the same evaluation procedure. Therefore please change the title of your manuscript accordingly upon revision; e.g., Evaluation of ECMWF IFS (v X.Y) operational model forecasts of aerosol transport in using ceilometer network measurements.

Response: We thank the editor for the reminder. We have revised the title of the manuscript to 'Evaluation of ECMWF IFS (version 41R1) operational model forecasts of aerosol transport by using ceilometer network measurements' in order to fulfill the requirement of the journal.

Response to reviewer #1

We thank reviewer #1 for the quick response and the comments. These comments were helpful for improving our manuscript. We have addressed the reviewer's comments on a point to point basis as below for consideration.

General comment:

The authors have compared attenuated backscatter profiles calculated from model simulation of the European Centre for Medium-Range Weather Forecast Integrated Forecast System (ECMWF-IFS) and ceilometer network measurements operated by the German weather service (DWD) over one year from September 2015 to August 2016. For this comparison it was necessary to convert the mass mixing ratios of 11 aerosols types of the model to attenuated backscatter described in detail in Section 3.1. This conversion involves a lot of assumptions, simplifications and uncertainties, and not surprisingly, the agreement with the ceilometers is not very strong. Given the complexity of the approach and the discrepancies in the results the benefit remains unclear. The ceilometer network in Germany is dense enough (and still increasing) to give a relatively complete picture of the vertical aerosol layering over the country. Although the paper is generally well written I am reluctant to support its publication unless the authors explain more convincingly the purpose of their investigation.

Response: The main concern of the reviewer is the large number "of assumptions, simplifications and uncertainties" used in the conversion procedure. We don't feel that this criticism is justified, otherwise, remote sensing (from ground and space) cannot be used for validation purposes at all. As remote sensing is relying on measurements of components of the radiation field, and models provide primarily physical properties (e.g. mass mixing ratios) conversion is an intrinsic feature of this kind of validation or comparison. In general the conversion of physical properties to optical properties is much better defined than the opposite direction, thus, in our case the uncertainties are comparably small: scattering theory (Mie or T-matrix approach) is generally accepted and if the microphysical properties are known (in our case prescribed or calculated from the model) the conversion is "exact". Open questions are discussed in our manuscript: Is the assumption of spherical particles correct and what is its influence on the "reality" (in our case the measurements)? Is the choice of the hygroscopic growth model relevant? In this context we have described the theoretical background and the inherent assumptions, so that the reader can understand what was done.

To determine the agreement or disagreement between observations and model output was the goal of our study. A key point was to find out if improvements with respect to the modeling of the hygroscopic growth and the consideration of particle shape can reduce the disagreement. We believe that this is a clear benefit of the study as it could help to create sort of a priority list for modifications of the model physics (is it worthwhile to spend efforts on a certain topic?). Moreover, as to our knowledge the use of the ceilometer network (an already existing routinely

24/7 working infrastructure) for these purposes has not been investigated before our paper can be a first step towards new applications of this infrastructure.

Detailed comments:

p. 3, line 10: explain GEMS

Response: We have now supplemented the information of GEMS (page 1, line 4; page 4, line 10-11).

p. 6, lines 8-9: Why does this not apply to ceilometers of DWD? Why discussing β_p when not used?

Response: It is because ceilometers of the DWD measure at 1064 nm which is not affected by the water vapor absorption. Nevertheless this topic should be mentioned as the majority of ceilometers are operating in the water vapor absorption band. A detailed description of the DWD ceilometers network is presented in section 2.2. We have recapped the measurement wavelength of DWD ceilometers to avoid confusion. In addition, we have removed the information of β_p error to avoid redundancy (page 9, line 13-14).

p. 10, line 2 ff: better rename CL (e.g. calibration factor instead of constant) as it is variable

Response: In the lidar community the term “lidar constant” is common, whereas operators of ceilometers use both terms synonymously. We agree that “calibration factor” better indicates that the value might be time-dependent. We believe that all scientists working in the lidar-field are aware of this fact even if they use “lidar constant”. Nevertheless we have clarified the reviewer’s concern in the revised manuscript (page 9, line 7-8).

p. 11, lines 19-21: re-phrase sentence (grammatically not correct)

Response: We have rephrased the sentence (page 14, line 9-10).

p. 12, line 15: 120 ceilometer profiles per which time span?

Response: Individual ceilometer profile is taken every 15s. In this study, we compare hourly averaged ceilometers data to model simulation. As a consequence, averages consider 240 ceilometer profiles at maximum. On the other hand, data contaminated by low clouds and precipitation are not considered in this study. The total least squares regression line is based only on intercomparisons when the hourly averaged data contains at least 120 ceilometer profiles (30 minutes of measurements). We have rephrased the sentence to avoid confusion (page 16, line 2-3).

p. 15, lines 5-6: is there any proof of this statement? (we learn that the presented IFS model results are very uncertain) Later the authors state that sea salt is probably over-estimated. Fig. 10a: the high backscatter between 00 and 06 UTC is not discussed/explained.

Response: We have now included references to support the fact that dust particle is a minor contributor to the aerosol abundance in Germany (page 22, line 11). The high backscatter from 00:00UTC to 06:00UTC is due to the present of cloud. We have supplemented the explanation on page 23, line 13-14.

p. 15, lines 26-27: The night-time mixing height is very likely even much lower than the mentioned 1.5 km. The phrase in parentheses does not support the statement outside.

Response: We mean that the maximum height (i.e. in the afternoon) of the mixing layer is usual below 1.5km during spring time. Of course, the mixing layer height could be lower during night time, but it does not contradict the statement. We have rephrased the sentence to avoid confusion (page 24, line 4-5).

Section 4.2: partly speculative, many unproven assumptions, not convincing.

Response: We have revised the section and provided more details from both model simulation and ceilometer measurement. In addition, we have rephrased the section to make it less speculative.

Response to reviewer #2

We thank reviewer #2 for careful reading our manuscript and the very detailed and helpful comments. They certainly helped us to improve the manuscript. We understand that the comments on the scientific content of the manuscript in general are positive, however, several clarifications are necessary. We hope the revised form of the manuscript has improved in all aspects and the manuscript is relevant to aims and scope of the journal. We have addressed the reviewer's comments on a point to point basis as below for consideration.

General comment

The paper "Evaluation of operational model forecasts of aerosol transport using ceilometer network measurements" aims at comparing the aerosol distribution forecasted by the CAMS-ECMWF aerosol model to measurements from a ceilometer network operative over Germany. The comparison covers one year (2015-2016). These type of model evaluations are very useful to highlight model errors and to improve the aerosol modeling and given that ceilometers are generally easier and cheaper to maintain than more complex lidar system, they could provide much needed extra information alongside more complete observations from network such as AERONET.

I think the paper needs mayor revisions before being accepted for publication. The major problem I see are the weak conclusions drawn from the comparison given the relative limited information that can be extracted from the ceilometer signal. Although these shortcomings are somehow acknowledged throughout the paper, a number of speculative conclusions are nevertheless attempted and this makes the overall results of the analysis somewhat unclear. Moreover, the number of assumption needed to compute the attenuated backscatter from the model are not always discussed in detail.

The language is generally clear throughout but it could be improved by some extra polishing.

Specific comments

Abstract Here and in the rest of the paper: for completeness it should be stated that the aerosol forecasts are produced within the Copernicus Atmosphere Monitoring Service (CAMS) using the aerosol module developed within the GEMS and MACC projects and coupled to the IFS.

Response: We have now included a better description of the model output used in this study (abstract and section 2.1).

line 2: The comparison is really using the mixing ratio from the IFS, not the backscatter profile, which was not available in the model cycle used in this work.

Response: We have now changed "aerosol backscatter profile" to a generic "aerosol profile" (a precise explanation is provided later in the paper) in order to avoid confusion. A more detailed description of the forward calculation for the conversion of aerosol mixing ratios to backscatter profiles is presented later in the manuscript.

line 8: "slightly" too vague, it does not really mean much here.

Response: We removed the word ‘slightly’ from the sentence (page 1, line 10).

line 18: not sure what to make of this: it does not make for a grand introduction to the work and downplays the analysis

Response: We removed the sentence from the abstract (page 2, line 1).

Introduction line 9-14: about the complexity of atmospheric modelling is perhaps better to provide a short discussion on the current status of aerosol modelling and sources rather than state that it is indeed a difficult problem

Response: We have revised the introduction to include a selection of relevant citations concerning the current status of aerosol modeling aerosol emission sources, and comparisons with observations (page 2, line 15 to page 3, line 11).

Section 2.1 Here it should be specified that the operational ECMWF forecasts do not provide any aerosol information. Only the forecasts provided by CAMS are produced by coupling an aerosol and chemistry module to the ECMWF IFS to provide analysis and forecasts of atmospheric composition It is not clear from this section which data are used in the comparison. Is it analysis fields? Or forecasts? If forecasts, at which lead time?

Response: In order to avoid the confusion, we have now revised the description and state clear that the aerosol simulation is provided by CAMS with the coupling of the aerosol and chemistry module to the ECMWF-IFS model. Daily forecast data are taken at 00:00 UTC each day, resulting a forecast lead time of 0-21 hours. This information is now included in the manuscript (page 4, line 9-10).

pag4, line 22: given that only results for wavelengths relevant for ceilometers are discussed, there is not point to show values for other wavelengths here. Also, the table could be restructured using two columns per optical property to show the values for the relevant wavelength, eliminating the need of copy and paste all the other information for each wavelengths.

Response: Although some of the wavelengths shown in the manuscript are not used in this study, they are relevant for other common ceilometers and aerosol lidar applications. Thus we believe that this information might be useful. Nevertheless, we followed the reviewer's comment and removed the other wavelengths from the description. In addition, we have also modified Table 2 and put the information of the other wavelengths in appendix (Table A1).

pag4, line 27: the horizontal resolution should be a Gaussian grid, not regular. The CAMS forecasts for CY41R1 should be at a spectral truncation TL255, roughly equivalent to a 0.7x0.7 degrees resolution. Please check the information.

Response: IFS is a spectral model, but in the Meteorological Archival and Retrieval System (MARS) at ECMWF, GRIB data is archived in one of the following spatial coordinate systems: Spherical Harmonics (SH), Gaussian Grid (GG) or Latitude/Longitude (LL). From this archive we retrieved the data as NetCDF files on a regular lat/lon grid. While the original model resolution is approximately 0.7° (360°/2/255), within MARS, the data is then transformed to a regular grid of 1°x1°. We have supplied the additional information in the manuscript (page 4, line 27-30).

pag4, line 29: in cy41R1 aerosol in IFS are not interactive with radiation and no explicit output of backscatter profile is provided. Hence the information about the assumptions in the optical properties used in IFS are not relevant here. Given that the computation of the backscatter profile is done off line using the aerosol mixing ratio from the model, the choices of refractive index and size distribution is entirely up to the user. The choices should be discussed in a separate sub section, and if the user wants to adopt the same values used in the IFS for the computation of the aerosol optical depth, it should be justified. Also this is the place to discuss further choices in the treatment of optical properties (e.g. hydrophilic growing factors and particle shape)

Response: The optical properties of aerosol are calculated offline from the model output of aerosol mass mixing ratios by assuming aerosol microphysical properties. Some of these properties are defined in the model, i.e. size bins, other properties are taken from external databases. We decided to adapt the aerosol microphysical properties used for aerosol optical depth calculation in the previous study (Morcrette et al., 2009), as it provide a rather complete overview and the resulting aerosol optical depths also agree well with measurements. In addition, we also performed some sensitivity tests, e.g. concerning the hydroscopic growth and the effect of nonspherical particles, to investigate the effects on especially lidar related aerosol optical properties. We follow the reviewer’s comment and moved the description of aerosol microphysical properties in new section (section 2.2).

pag4, line 26: modal radius and limits of integration over the size distribution

Response: Revised according to reviewer's comment (page 5, line 32).

pag 5, line 4: this has to be explained a bit more carefully because it might be relevant given the results shown later on.

Response: A more detailed explanation is included in the manuscript (page 6, line 10-11).

section 3.1 Not clear: the title of the section says attenuated backscatter but from the text it looks like the computed quantity here is the true layer backscatter.

Response: Obviously this section was confusing so that we emphasize at the end of Section 3.1 (page 11, line 8-10) that attenuated backscatter is calculated. Input for this calculation is - among others - the particle backscatter coefficient. The definition of attenuated backscatter is provided in Eq. 2.

pag 7, line 20: unusual terminology, isn't it equation 7 just the definition of the mass extinction coefficient?

Response: In principle the reviewer is right: This is indeed a "mass extinction coefficient". On the other hand a "mass extinction coefficient" usually refers to the "total" size distribution of the particles, whereas here a size range according to the specific bins is considered. So, different mass extinction coefficients are existing. As readers also might be used to that term we have followed the reviewer's suggestion and revised the terminology (page 10, line 16-17).

section 3.2 pag9, line 2: define slow. Will impact a full year of data like in this work?

Response: The DWD ceilometers are calibrated routinely whenever possible (i.e., adequate weather conditions are prevailing). Thus, changes are monitored and can be considered. Details of the calibration are given in the following paragraph (page 12, line 1-12). In this context it is indeed irrelevant whether these changes are "slow" or not. Consequently we rephrased this sentence. (page 11, line 21-22).

pag 10, line 10: 'sky-condition-index' and 'cloud-base-height' not defined. Not clear how they are used, is it to exclude data not relevant for aerosol comparisons?

Response: Those are data quality flags provided by the proprietary software of the ceilometers which are used to filter data contaminated by rain, fog, snow and low level clouds. The definitions of those flags are now provided in the manuscript (page 12, line 16 to page 13, line 2).

pag 10, line 11: If mentioned it is probably useful to have an idea of how much this variation in the accuracy of the calibration constant actually is.

Response: The lidar constant C_L is routinely calibrated as mentioned in the previous paragraph. Therefore, possible changes with time can be observed. The typical error of individual calibration is 15-20 %, while the actual error is smaller due to the temporal smoothing. The monthly variation of C_L is usually less than 5 % and the annual variation is 10-15 %.This information is now included in the manuscript (page 12, line 10-12).

section 4 pag 10, lines 19-25: not clear

Response: We have rephrased the corresponding paragraph: our message is that even if β_p of an elevated layer agrees, attenuated backscatter may disagree if there are differences (model vs. observations) in the atmosphere below(page 13, line 8-14).

pag 10, line 27: as already outlined: not clear which model data have been used. Forecast fields? Analysis?

Response: This issue has been addressed according to earlier comment.

pag 10, line 29: confusing, why here 2 km maximum height is used and few lines before 1 km was mentioned?

Response: We compare β^* averaged from 0.2 km to 1 km, while the cloud filtering criterion of low level cloud is ‘2 km’. In principle the reviewer is right: it would be sufficient to exclude measurements with clouds in the range where we determined β *. However, to be on the safe side (in the case of errors of the cloud bottom height) we used a cloud filter criterion of 2 km instead of 1 km. Moreover, this criterion allows us to use the same data sets for intercomparisons of profiles as discussed later in the paper. These profiles should at least have a vertical extent of 2 km, otherwise their benefit for aerosol studies is in general limited (e.g., radiation budget). As a consequence, we have rephrased the sentence to avoid confusion (page 13, line 19).

section 4.1 pag 11, line 10: well perhaps a look at some of those situations might help to give some clue. Aren't the events in December and at the beginning of April 2016 the dust advection cases discussed later on?

Response: We have now referred the readers to section 4.1.2 and 4.2 for more detailed analysis (page 13, line 31).

pag 11, line 15: how does it compare to the uncertainty expected from the measurements at each site? Perhaps a table with the annual mean and some measure of uncertainty and dispersion of the data at each site gives a clearer picture.

Response: We followed the reviewer's comment and added a table to summarize the annual mean and the uncertainty of all sites (Table 3).

pag12, line 1: here it is meant larger or smaller than sigma in absolute value I guess

Response: It means the absolute difference between model and observation smaller or larger than the standard deviation obtained from the statistic. The standard deviation of the difference for each site is included in the new Table 3. In the revised version the notation for absolute values has been added (page 14, line 15).

pag 12, line 21-25: if it is the case that sea salt is largely overestimated, there should be a discussion showing the contribution of all aerosol types to the total AOD and total mass for each site, not only the contribution to the backscatter.

Response: Here we just listed some possible reasons for the discrepancy between model and observation. It can be related to the assumed optical properties of aerosols or uncertainty related to the emission and transportation of aerosols in the model. As the focus of the manuscript is the comparison of backscatter data, we have only added a brief summary of the contribution of sea salt with respect to the AOD (following the reviewer's suggestion). The annual averaged sea salt contribution to the total AOD is ranging from 21% (Görlitz) to 37% (Elpersbüttel). The information is supplemented to the manuscript (page 17, line 4 to page 18, line 3).

section 4.1.1 this is really relevant only if the influence of the overestimation in total sea salt amount and in the choices of optical properties are not the main reason behind the discrepancy (which most likely are it seems). Moreover given the difficulties highlighted throughout the test (e.g. pag 13 line 10) and the relatively small contribution that this correction brings, this section could be significantly reduced.

Response: We understand the reviewer's concern that the model errors might have a larger impact on the comparison. However, we could not solve this from the forward operator perspective. Therefore, we tried to quantify another major source of error - hydroscopic growth. As we have shown in the manuscript the influence of using a better hydroscopic growth database would result in a 22% reduction of sea salt backscatter. Considering sea salt contributes over 50% of the total backscatter, a 22% reduction of sea salt backscatter would reduce the total backscatter by more than 10%. With these information the readers can judge by themselves which priority they give to this topic when thinking about improvements of the model, so we think this section is useful. Nevertheless, in response to the reviewer's comment, we have reduced the discussion in this section.

section 4.1.2 pag 13, line 26: not necessarily. Nonsphericity might have a non negligible contribution to the lidar backscatter signal, but for flux computations, e.g. in a typical radiation code of a climate or NWP model, the impact is often small (e.g. Räisänen et al. 2012 https://doi.org/10.1002/qj.2084)

Response: The statement of the reviewer is in agreement to our manuscript (page 20, line 19-20). We have explicitly mentioned that the nonsphericity of particles has only a small impact on the extinction. However, the effect on backscatter is quite large (up to 45%). Insofar the first sentence should not be misunderstood as "important role for all optical properties". We changed this to "lidar related optical properties" (page 20, line 12-13).

pag 14, line 7: I think that it's clear that the vertical profile is not affected by the choice of particle shape.

Response: We removed the sentence 'independent of the numerical treatment of the particle shape' (page 21 line 7).

pag 14, line 11: The choice of size distribution/refractive index also plays a role.

Response: We have now supplemented the information of other possible influences (page 21 line 10-11).

section 4.2 pag 15, line 14: it could be nice to see another one or two sites since Elpersbuettel is at the edge of the event and more susceptible to errors in the plume location.

Response: We have added another example of Alfeld, 250 km south of Elpersbüttel, to illustrate the arrival and the temporal development of the dust episode influences (page 26 line 7-11). Due to the length of the manuscript, we have moved these plots to the appendix.

pag 15, line 16: why? from the IFS only the mass mixing ratio is used, there is no need to be consistent with other assumptions here. If the non spherical assumption brings results slightly closer to the observations, then perhaps this should be used.

Response: The nonspherical assumption does not show a significant impact on the relative attenuated backscatter profile. Therefore, it does not affect the interpretation of the dust layer. However, we follow the reviewer's comment and now used the nonspherical assumption for these plots (page 23, line 3-4 and Fig. 10-13).

pag 15, line 17-18: "it seems". It should be discussed better

Response: We have rephrased the wording to make it less speculative (page 23, line 6).

pag 15, line 19: plotting the two profiles (model-observed) on the same chart will help the comparison

Response: We followed the reviewer's comment and include the averaged ceilometer attenuated backscatter profiles in Fig. 10b, 11b and 13b.

pag 15, line 26: why this assumption if it cannot be proven?

Response: This is not an assumption but a conclusion from the model result. We have rephrased the sentence to avoid confusion (page 34, line 4-5).

pag 15, line 31: again, perhaps showing the model profile broken down in the 5 aerosol species cloud help

Response: The time series of the contribution of particle backscatter for the five aerosol types is shown in a new Fig. 12 for a better interpretation of temporal development of the dust layer.

pag 15, lines 33-34 pag 16, lines 1-2: too speculative, does not add to the general discussion.

Response: In this point we disagree with the reviewer: We believe that it is important to show the limits of the validation. In the case of low level clouds that cannot be penetrated by the ceilometer measurements, information of the atmosphere above the clouds is not available. This is an inherent problem of all lidar/ceilometer measurements.

pag 16, line3: not easy to see from the plot.

Response: We have now revised the figures and show both ceilometer and model profile in the same plot (Fig. 10b, 11b and 13b.).

pag 16, line 4-6: from the ceilometers alone not much can really be said. Does the model speciation show the decrease in dust mixing ratio?

Response: The model simulation shows the dust concentration gradually decreased during the day and finally disappeared at 18-21 UTC. As there are already too many figures in the manuscript, we decide not showing the aerosol speciation particle backscatter profile. However, we have revised the sentence to avoid any confusion (page 25, line 9-12).

pag 16, lines 8-11: quite speculative and not much relevant

Response: We have removed these sentences from the manuscript.

pag 16, lines 11-20: it could be interesting to see it. Otherwise there is not much point in mentioning it.

Response: We have now included the measurement and model simulation results from Alfeld, about 250km south of Elpersbüttel, to illustrate the arrival and the temporal development of the dust episode. Due to the length of the manuscript, we have moved these plots to the appendix.

pag 16, lines 21-26: rather inconclusive paragraph. If the discussion would stick to what can be seen from the ceilometer without trying to extrapolate too much beyond (probable hieght above cloud layers, uncertain arrival and dissolution of the aerosol plume, speciation), I think the interesting result to highlight is that the main feature of such an event can be captured and compare reasonably well with the model fields.

Response: We have revised the whole paragraph to avoid over interpret the model and observation data (page 26, line 16-19).

Evaluation of ECMWF IFS (version 41R1) operational model forecasts of aerosol transport by using ceilometer network measurements

Ka Lok Chan[1,2], Matthias Wiegner[1], Harald Flentje[3], Ina Mattis[3], Frank Wagner[3,5], Josef Gasteiger[4], and Alexander Geiß[1]

[1]Meteorological Institute, Ludwig-Maximilians-Universität München, München, Germany
[2]Remote Sensing Technology Institute, German Aerospace Center (DLR), Oberpfaffenhofen, Germany
[3]Department of Research and Development, Meteorological Observatory Hohenpeißenberg, German Weather Service (DWD), Hohenpeißenberg, Germany
[4]Aerosol Physics and Environmental Physics, University of Vienna, Austria
[5]now at: Institute for Meteorology and Climate Research, Karlsruhe Institute of Technology, Eggenstein-Leopoldshafen, Germany

Correspondence: Ka Lok Chan (ka.chan@dlr.de)

Abstract. In this paper, we present a comparison of ~~European Centre for Medium-Range Weather Forecast Integrated Forecast System (ECMWF-IFS) model simulation of aerosol backscatter~~ model simulations of aerosol profiles with measurements of the ceilometer network operated by the German ~~weather service~~ Weather Service (DWD) over 1 year from September 2015 to August 2016. The aerosol forecasts are produced by the Copernicus Atmosphere Monitoring Service (CAMS) using the aerosol module developed within the Global and regional Earth-system Monitoring using Satellite and in-situ data (GEMS) and Modelling Atmospheric Composition and Climate (MACC) projects and coupled into the European Centre for Medium-Range Weather Forecast Integrated Forecast System (ECMWF-IFS). As the model output provides mass mixing ratios of different types of aerosol whereas the ceilometers don't, it is necessary to determine a common physical quantity for the comparison. We have chosen the attenuated backscatter β^* for this purpose. The β^*-profiles are calculated from the mass mixing ratios of the model output assuming the inherent aerosol microphysical properties. Comparison of the attenuated backscatter ~~,~~ averaged between an altitude from 0.2 km (typical overlap range of ceilometers) and 1 km ~~, showed slightly larger valuesfrom the model~~in general shows similar annual average values. However, the standard deviation of the difference between model and observation is in 8 out of 12 sites larger than the average.

To investigate possible reasons for the differences, we have examined the role of the hygroscopic growth of particles and the particle shape. Our results show that using a more recent particle growth model would result in a ∼22 % reduction of particle backscatter for sea salt aerosols, corresponding to a 10 %-reduction of the total backscatter signal on average. Accounting for ~~non-spherical~~ nonspherical dust particles in the model would reduce attenuated backscatter of dust particles by ∼30 %. As the concentration of dust aerosol is in general very low in Germany, a significant effect on the total backscatter signal is restricted to dust episodes. In summary, consideration of both effects ~~tend~~ tends to improve the agreement between model and observations, but without leading to a perfect consistency.

In addition a case study was conducted to investigate strong Saharan dust event was investigated to study the agreement of the spatiotemporal distribution of particles. It was found that for a dust episode in April 2016 the arrival time of the dust layer and its vertical extent very well agree between model and ceilometer measurements for several stations. However, due to the large set of parameters characterizing the aerosol distribution and the complexity of the ceilometer retrieval an automated and quantitative comparison scheme for β^*-profiles is still missing. Consequently, the representativeness of the case study remains open. This underlines the potential of a network of ceilometers to validate the dispersion of aerosol layers.

1 Introduction

Aerosols are an important constituent of the atmosphere playing a key role in the Earth's climate and weather system. They influence the Earth's radiation budget directly by absorbing and scattering of radiation and indirectly by providing nuclei for cloud condensation. The chemical and physical properties of aerosols depend on their composition and sources. In recent decades, an increasing amount of anthropogenic aerosols is released into the atmosphere which makes it one of the largest uncertainties in assessments of climate change (IPCC, 2012). Numerous studies have been conducted in the recent decades to investigate the relationship between aerosols, air quality, weather and climate (Jones et al., 2001; Stier et al., 2005; Lohmann et al., 2007; Benedetti et al., 20 These studies mostly rely on model simulations. However, atmospheric processing of aerosols is quite complex, and their physical and chemical properties are highly variable , and cannot be easily characterized and parameterized. In addition, the emission sources of aerosols are not well estimated . Thus, in space and time. Thus, simplifications and assumptions are usually required for numerical weather prediction (NWP) and assessments of climate changeassumptions are required with respect to the physics and chemistry of aerosols and the computations of their radiative properties.

The current state of the description of radiative properties of particles in numerical models is elaborated e.g. by Baklanov et al. (2014). The influence of the description of particle microphysics, including their mixing state, hygroscopic growth and shape, on simulated aerosol optical properties was discussed e.g. in detail by Curci et al. (2015). Numerical simulations of atmospheric composition require meteorological data and chemical emission inventories as input. Emission inventories of anthropogenic pollutants can be estimated through the 'bottom-up' or 'top-down' method. The former one relies on statistics of local information, such as road graph, industry location, population density, and electricity consumption, together with appropriate emission factors. The latter one uses observations as input and disaggregated to different emission sectors by means of local statistical indicators (van der Gon et al., 2012). Due to the rapid changes of sources, emission inventories might be outdated in specific regions introducing large uncertainties in the model. Moreover, physical and chemical processes in the atmosphere are parameterized in models due to the intricacy of these processes, leading to additional uncertainties. As a consequence, validation of forecasts model output against observational data becomes increasingly important(e.g., Binietoglou et al., 2015; Cuevas et al., 2015;

The relevance of validation is documented by the establishment of international activities, e.g. the Air Quality Model Evaluation International Initiative (AQMEII, Rao et al. (2011)) when up to 20 groups provided model simulations of – among others – particulate matter. Common to almost all validation activities – except for in-situ-measurements of mass concentrations

– is that they require the transformation of prognostic variables of the model, e.g. mass mixing ratios of a number of aerosol components, to variables that can be measured. These are typically optical properties of the aerosols. Validation studies relying on in-situ measurements of near surface concentrations, e.g. from the Airbase and EMEP-networks, were conducted e.g. by Solazzo et al. (2012); Im et al. (2015). Measurements of aerosol optical depth (AOD) are mainly based on AERONET. Balzarini et al. (2015) compared AOD at 12 AERONET sites and in-situ measurements from ground-based networks to investigate the performance of two chemical mechanisms of WRF-Chem (Grell et al., 2005; Fast et al., 2006). In the framework of AQMEII-2 modeled single scattering albedo, asymmetry parameter and AOD were also compared to AERONET data (Curci et al., 2015). AOD and Angström exponents from AERONET as well as AOD from spaceborne measurements were used for validation in the framework of the MACC-II reanalysis project (Cuevas et al., 2015). Investigations in how far range resolved measurements from active remote sensing systems can serve for model validation has been conducted in the last few years only. A combination of EARLINET and AERONET data for the Lidar-Radiometer Inversion Code (LIRIC, Chaikovsky et al. (2016)) was used by Binietoglou et al. (2015) for ten selected stations to investigate the accuracy of four dust transport models. Siomos et al. (2017) also used LIRIC and focused on the validation of aerosol mass concentration profiles for 22 cases over Thessaloniki, Greece. Mona et al. (2014) performed an intercomparison on the basis of extinction coefficient profiles from EARLINET data at Potenza, Italy, and the BSC-DREAM8b model covering 310 cases out of 12 years. These studies demonstrated impressively that the exploitation of range resolved measurements offers new perspectives for validation.

Quantitative range resolved aerosol parameters can be obtained from advanced lidar measurements. These lidar systems are ~~very expensive~~ however expensive in invest and maintenance, and continuous operation is ~~still an exception at the current state-of-the-art. On the other hand, ceilometers can be considered as simple single wavelength backscatter lidars with low energy consumption. Because~~ only slowly developing. For these reasons, ceilometers might be a new option, though they are only simple single-wavelength low energy backscatter lidars. On the other hand they are eye-safe ~~they~~ and can be operated continuously and fully automated, therefore making them suitable for setting up extended networks. In recent years, many ~~of the~~ synoptic observation stations have already been equipped with ceilometers and the number is still growing. Although ceilometers were originally designed for cloud ~~heights detection~~ height detection only, recent studies show ~~the~~ that ceilometers are also able to measure aerosol profiles ~~(Flentje et al., 2010; Wiegner and Geiß, 2012; Madonna et al., 2015)~~(Flentje et al., 2010; Wiegner and Gei If ceilometers are calibrated the primary output is the so-called attenuated backscatter β^*. ~~This quantity can be converted to~~ Inversion of the signals provide the particle backscatter coefficient β_p if the lidar ratio S_p is known. As β_p in the infrared spectral range is rather insensitive to errors of the lidar ratio S_p this is typically not an issue. ~~.~~In contrast, the derivation of ~~the~~ aerosol extinction coefficients α_p may be subject to large uncertainties due to an actually unknown lidar ratio. As a consequence, β^* or β_p are candidates for validating aerosol profiles derived from NWP-models. However, to our knowledge this approach has not yet been applied.

In this study, for the first time a comparison of aerosol profiles provided by the operational Integrated Forecast System of the European Centre for Medium-Range Weather Forecast (ECMWF-IFS) with long term measurements of the ceilometer network measurements operated by the German ~~weather service~~ Weather Service (DWD) is presented. IFS is quite relevant as it is often used to provide boundary conditions for regional models. In section 2, the ceilometer data and the aerosol ~~parameterizations~~

~~of~~ description in the model are described. ~~As the model predicts mass mixing ratios of different types of aerosols whereas the ceilometers provide backscatter-related quantities, the first step must be the selection of a common physical quantity for the comparison. It is described~~ The concept used for the validation is discussed in section 3. The intercomparison discussed in section 4 comprises ceilometer measurements of one year (from ~~1.~~ 1 September 2015 to ~~31.~~ 31 August 2016) at 12 different stations in Germany and includes investigations of the importance of the numerical description of the hygroscopic growth ~~of particles and the particle shape ,~~ and shape of the particles. Moreover, the agreement of the spatiotemporal distribution of dust particles during a Saharan dust event is discussed. A summary and suggestions for further studies conclude the paper.

2 Basis of the intercomparison

The comparison of 'aerosol profiles' derived from weather forecast models and retrieved from ceilometer measurements suffers from the fact that models and measurements do not provide the same physical quantity. In this section the output of the IFS and the ceilometers is described. This constitutes the basis for the determination of a common quantity for the intercomparison.

2.1 ECMWF-IFS: aerosol description

The European Centre for Medium-Range Weather Forecast Integrated Forecast System (ECMWF-IFS) is a comprehensive Earth-system model. ~~The model is used for forecasts and analysis~~ An aerosol and chemistry module is coupled to the ECMWF-IFS by the Copernicus Atmosphere Monitoring Service (CAMS) to provide analysis and forecasts of atmospheric composition (Buizza et al., 1999; Rabier et al., 2000; Bechtold et al., 2008; Drusch et al., 2009; Dutra et al., 2013). In this study, daily forecast data are taken at 00:00 UTC resulting a forecast lead time of 0 - 21 hours. In the framework of ~~GEMS, aerosols~~ Global and regional Earth-system Monitoring using Satellite and in-situ data (GEMS), concentrations of aerosol compounds were included as new prognostic variables into IFS (Morcrette et al., 2009; Benedetti et al., 2009). The parameterization of aerosol physics is mainly based on the concept of the LOA/LMD-Z model (Boucher et al., 2002; Reddy et al., 2005). ~~The aerosol microphysics follows the sectional representation of the size distribution (e.g., Zhang et al., 1999; Mann et al., 2012).~~ Tropospheric aerosols are introduced in the model including two natural types, sea salt and dust, and three other types with significant anthropogenic contribution, i.e., sulfate, organic matter and black carbon. Stratospheric and volcanic aerosols are not considered in the present version.

The emission of sea salt and dust is controlled by the wind speed at a height of 10 m. Following the findings of Engelstaedter and Washington (2007), it was suggested by Morcrette et al. (2008) to also consider the gustiness of the wind. The sources for the anthropogenic aerosols are taken from external emission inventories, i.e., the Emission Database for Global Atmospheric Research (EDGAR, 2013), the Global Fire Emission Database (GFED, van der Werf et al. (2010)) and the Speciated Particulate Emission Wizard (SPEW) were used in the simulation. A detailed description of the sources of aerosols can be found in Dentener et al. (2006).

The above mentioned five aerosol types are further subdivided: natural aerosols are categorized into three different size bins each, whereas carbonaceous aerosols are differentiated into hydrophobic and hydrophilic particles. Sulfur is presented in the model in two forms, sulfur dioxide (SO_2) and sulfate (SO_4), the former one was assumed in gas phase while the latter is assumed in particulate phase. In total, the mass mixing ratios m of 11 different aerosol types (see Table 1) are introduced as prognostic variables in the model. It is

Mass mixing ratio of these 11 types of aerosols are provided with a temporal resolution of 3 hours. The horizontal resolution of the IFS model (version 41R1)is original model output is approximately $0.7° \times 0.7°$. The data is then transformed to one of the following spatial coordinate systems: Spherical Harmonics (SH), Gaussian Grid (GG) or Latitude/Longitude (LL). From this archive we retrieved the data on a regular Latitude/Longitude grid with $1° \times 1°$, while the resolution. The vertical dimension of the model is separated into 60 pressure-sigma levels. Optical properties of aerosol, e.g., extinction coefficient, aerosol optical depth and backscatter coefficient, are not included in the output of the model, but calculated offline from the model output of aerosol mass mixing ratio. A more detailed description of the treatment of the aerosols can be found in Morcrette et al. (2009).

2.2 Aerosol microphysical properties

To determine the interaction between aerosols and radiation, the optical depth properties of each type is are calculated for the short-wave and long-wave spectral range. In this context also the change of the optical properties with relative humidity is considered. All calculations are based on the Mie theory even if the particles of a specific aerosol component are most likely non-spherical (e.g. , dust)In this study, we adapted the aerosol microphysical properties assumed in the previous study (Reddy et al., 2005), as the resulting aerosol optical depths were reported to agree well with observations (Morcrette et al., 2009). A brief description of the aerosol micropyhsical properties relevant for this study is presented in the following.

The particle size distribution is assumed to be a lognormal distribution lognormal with three parameters: $\sigma_{g,i}$ as the 'geometric standard deviation', i.e., the width of the distribution, $r_{0,i}$ as the modal radius, and N_i as the total number concentration of particles of mode i. Thus, a the size distribution (with r as the particle's radius) consisting of k modes is described by Eq. 1

$$N(r) = \sum_{i=1}^{k} \frac{N_i}{\sqrt{2\pi} \cdot \ln\sigma_{gi} \cdot r} \cdot \exp\left\{ -\left(\frac{\ln r - \ln r_{0i}}{\sqrt{2} \cdot \ln\sigma_{gi}} \right)^2 \right\} \tag{1}$$

with normally $k \leq 3$.

In IFS, all All aerosol types except sea salt are assumed to be have a mono-modal lognormal distribution defined according to Eq. 1 (k=1). Only for sea salt, a bi-modal lognormal distribution is assumed (k=2). The parameters σ_g and r_0 characterizing each aerosol type are listed in Table 1. They are based on Reddy et al. (2005) and valid for dry particles.

For the sulfate, organic matter and black carbon aerosol type types $\sigma_g = 2.0$ is selected and the modal radii r_0 are 0.0355, 0.0355 and 0.0118 μm, respectively (Boucher and Anderson, 1995; Köpke et al., 1997). The microphysical properties of hydrophilic and hydrophobic carbonaceous aerosols are assumed to be the same.

Dust aerosols are also described by a mono-modal lognormal size distribution with $r_0 = 0.29\,\mu$m and $\sigma_g = 2.0$ (Guelle et al., 2000), but split into three size bins. The limits are 0.03 - 0.55 μm (fine mode), 0.55 - 0.9 μm (accumulation mode) and

0.9 - 20.0 μm (coarse mode), respectively. These boundaries are chosen so that approximately 10, 20 and 70 % of the total mass of the aerosols are in each of the size bins (Morcrette et al., 2009).

Sea salt aerosols as the second class of natural aerosols are also represented by three size bins. For dry sea salt aerosol, their limits are slightly different and set to 0.015 μm, 0.251 μm, 2.515 μm and 10.060 μm. In contrast to the dust aerosols, a bimodal lognormal with r_0 = 0.1002 μm and 1.002 μm and σ_g = 1.9 and 2.0 (O'Dowd et al., 1997) is assumed. The number concentrations N_1 and N_2 of the first and second mode are 70 and 3 cm^{-1}, respectively.

Table 1. Microphysical properties and selected optical properties of dry aerosols as used in the model.

Aerosol Type	Wavelength (λ, nm)	Density (ϱ_p, g/cm^3)	Modal Radius (r_0, μm)	Geometric Standard Deviation (σ_g)	Refractive Index (n)	Single Scattering Albedo (ω_0)	Specific Extinction Cross Section (σ_e^*, m^2/g)	Lidar Ratio (S_p, sr)
Sea Salt (bin 1)[a]	1064	2.160	0.1002,1.0020[c]	1.9,2.0[c]	1.5156-0.0002i	1.00	0.55	21.7
Sea Salt (bin 2)[a]	1064	2.160	0.1002,1.0020[c]	1.9,2.0[c]	1.5156-0.0002i	1.00	0.62	10.0
Sea Salt (bin 3)[a]	1064	2.160	0.1002,1.0020[c]	1.9,2.0[c]	1.5156-0.0002i	0.99	0.18	18.2
Dust (bin 1)[b]	1064	2.610	0.2900	2.0	1.4800-0.0006i	1.00	1.50	78.6
Dust (bin 2)[b]	1064	2.610	0.2900	2.0	1.4800-0.0006i	1.00	1.61	48.6
Dust (bin 3)[b]	1064	2.610	0.2900	2.0	1.4800-0.0006i	0.99	0.44	13.4
Organic Matter	1064	1.769	0.0355	2.0	1.5068-0.0000i	1.00	0.77	34.2
Black Carbon	1064	1.000	0.0118	2.0	1.7500-0.4500i	0.08	3.90	168.3
Sulfate	1064	1.769	0.0355	2.0	1.5068-0.0000i	1.00	0.77	34.2

[a] Sea salt aerosols are represented in the model by three size bins with the bin limits set to 0.015-0.251 μm (bin 1), 0.251-2.515 μm (bin 2) and 2.515-10.060 μm (bin 3).
[b] Dust aerosols are represented in the model by three size bins with the bin limits are set to 0.03-0.55 μm (bin 1), 0.55-0.90 μm (bin 2) and 0.90-20.00 μm (bin 3).
[c] A bimodal lognormal size distribution is assumed for sea salt aerosols, with r_0=0.1002 μm and 1.002 μm and σ_g=1.9 and 2.0. The number concentrations N_1 and N_2 of the first and second mode are 70 and 3 cm^{-1}, respectively.
Note that density of hydrophilic aerosol changes with hygroscopic growth of particle.

The refractive index of sea salt is assumed to be wavelength independent (Shettle and Fenn, 1979). For all other aerosol types a wavelength dependence is assumed and tabulated for 44 wavelengths between λ=0.28 μm and 4.0 μm, with values taken from Boucher and Anderson (1995); Köpke et al. (1997) and Dubovik et al. (2002). ~~In Table 1 only values at 355 nm, 532 nm, 550 nm, 910 nm and~~ The aerosol microphysical and optical properties at 1064 nm~~are given, the latter two as they are the most relevant wavelengths for ceilometer applications, whereas the short wavelengths are relevant for aerosol lidar applications including satellite missions (CALIPSO, EarthCARE)~~, the wavelength of the ceilometers of the DWD-network, are listed in Table 1. Other relevant wavelengths for ceilometer and lidar applications are listed in Table A1 in the appendix.

In case of hygroscopic growth of particles, their microphysical properties change. Typically this effect is parameterized by an increasing modal radius ~~of the lognormal~~ and limits of integration over the size distribution, whereas the width of the distribution σ_g is assumed to remain unchanged. The latter approximation is certainly a simplification, but frequently used. ~~In the IFS model, hygroscopic~~ Hygroscopic growth is considered for sulfate, hydrophilic organic matter and sea salt, see Fig. 1. It is parameterized by growth factors, defined as the ratio between the radius of the wet and dry particle (r/r_{dry}) and taken from the OPAC database (Hess et al., 1998). For sulfate and hydrophilic organic matter the same factors are used. Especially for a relative humidity above 70 % the growth is strong whereas no growth is assumed when the relative humidity is below 30 %. The refractive index n and density ϱ of wet particles is taken from a look up table with mixing rules following Hess et al. (1998).

To reduce computational time, the optical properties of hygroscopic aerosols are pre-calculated for 12 discrete relative humidity levels (0, 10, 20, 30, 40, 50, 60, 70, 80, 85, 90 and 95 %) and stored in a look-up table. It is important to note that

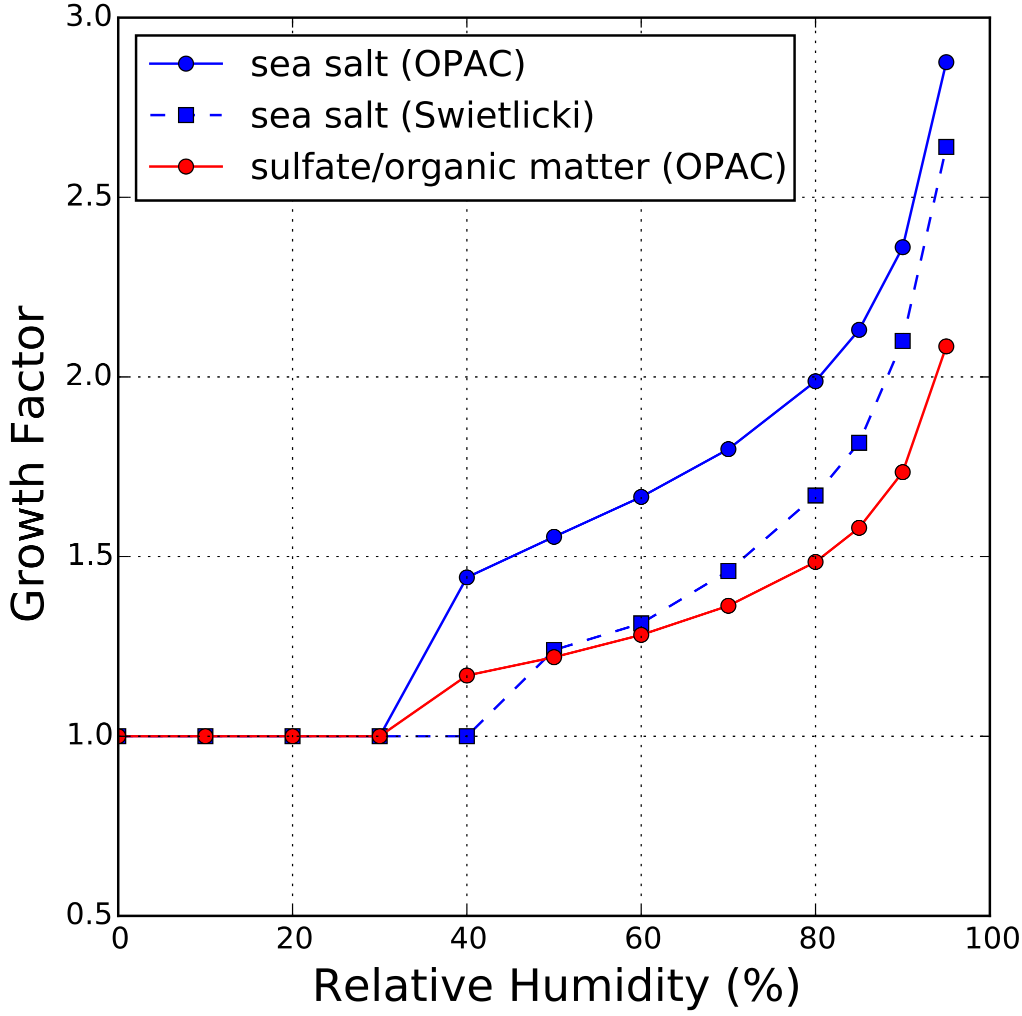

Figure 1. Hygroscopic growth factors of particle radius of sea salt, sulfate and hydrophilic organic matter aerosols as a function of relative humidity. Sulfate and hydrophilic organic matter share the same growth factor in the model (red curve). Growth factors of sea salt obtained from Swietlicki et al. (2008) are also shown for reference.

sea salt aerosols are emitted and transported as wet aerosols in the model with properties equivalent to 80 % relative humidity. Subsequently, the model reported mass mixing ratios of sea salt are converted back to dry aerosolsby applying the inverse of the growth factor. This conversion is achieved by dividing the model reported mass mixing ratios by the mass growth factor at 80 % relative humidity. The hygroscopic growth effect is then applied to the dry sea salt aerosols to determine the extinction and backscatter coefficientactual optical properties.

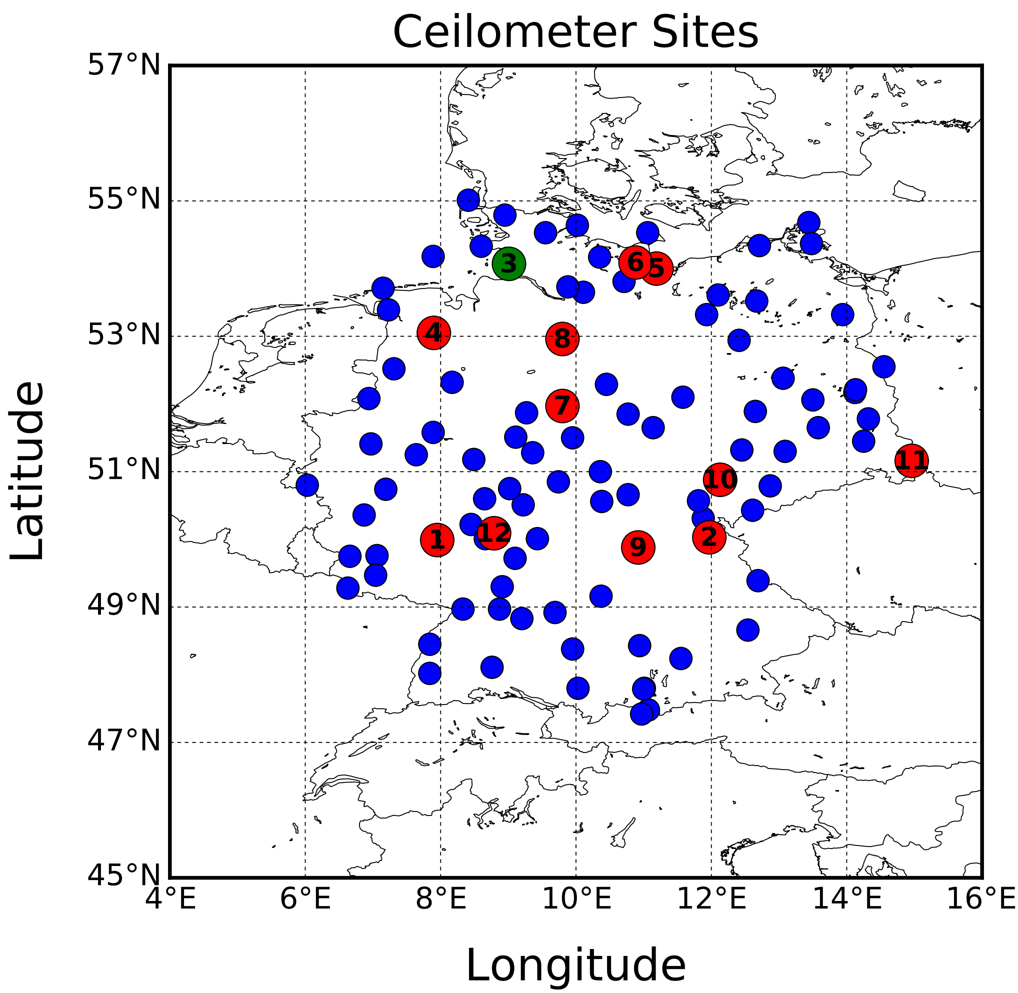

Figure 2. Location of the German weather service ceilometer sites as on end of 2017. The red spots indicate the ceilometer sites within 20 km of IFS model grid point while the blue markers represent the rest of the network. Note that some of the sites are not in operation during the period of study and therefore not included in this study. Elpersbüttel (see section 4) is indicated in green. More detailed information of the ceilometer sites can be found in Table 2.

In recent years, DWD has equipped a number of synoptic observation stations with Lufft (previously Jenoptik) ceilometers (CHM15k) to establish a ceilometer network (www.dwd.de/ceilomap). By the end of 2016, 100 ceilometers are put into operation in Germany. The locations of the ceilometer sites are indicated in Fig. 2. The ceilometer network is still expanding in order to have a better spatial coverage. The ceilometers are eye-safe and fully-automated systems which allow unattended operation on a 24/7 basis (Wiegner et al., 2014). Thus they are especially They are suitable for monitoring aerosol layers (e.g., volcanic ash, see Flentje et al., 2010; Emeis et al., 2011), validation purposes (e.g., volcanic ash, see Flentje et al., 2010), validation of meteorological and chemistry transport models (see e.g. Baklanov et al., 2014)(see e.g. Emeis et al., 2011), and are foreseen for data assimilation (e.g., Wang et al., 2014; Geisinger et al., 2017).

The CHM15k-ceilometer is equipped with a diode-pumped Nd:YAG-laser emitting laser pulses at 1064 nm. The typical pulse energy of the laser is about 8 μJ with a pulse repetition frequency of 5 - 7 kHz. The laser beam with divergence of $<300\,\mu$rad is emitted off-axis to the receiving telescope with a field of view of 450 μrad. Backscattered photons are collected by the telescope through a narrow band interference filter and measured by an avalanche photodiode running in photon counting mode. The received backscatter signals are stored in 1024 range bins with a resolution of 15 m, the temporal resolution is set to 15 s. The signals are corrected for incomplete overlap by a correction function provided by the manufacturer. As ceilometers are single-wavelength backscatter lidars the received signals follow the well known lidar equation. Calibration is required to retrieve quantitative results.

For the intercomparison of ceilometer measurements and modeled aerosol profiles we only consider sites within 20 km from a model grid point. This criterion results in a selection of 12 stations. Their location (latitude, longitude, altitude) together with their distance from the nearest IFS-grid point are summarized in Table 2.

Ceilometer sites within a distance of 20 km to the nearest IFS model grid point, altitude is given in meters above mean sea level, the distance to the nearest model grid point (in km) is given in the 5. column. No. Site Latitude (°N) Longitude (°E) Altitude (m) Distance (km) 1 Geisenheim 49.9866 7.9551 110 3.8 2 Wunsiedel 50.0316 11.9745 622 4.0 3 Elpersbüttel 54.0692 9.0105 3 7.8 4 Friesoythe 53.0500 7.9000 6 8.7 5 Boltenhagen 54.0027 11.1909 15 12.5 6 Pelzerhaken 54.0893 10.8773 1 12.7 7 Alfeld 51.9644 9.8072 144 14.1 8 Soltau 52.9605 9.7930 76 14.2 9 Bamberg 49.8743 10.9206 240 14.5 10 Gera 50.8813 12.1289 311 16.2 11 Görlitz 51.1633 14.9531 240 18.0 12 Offenbach 50.0894 8.7864 121 18.1

3 Concept of intercomparison

As mentioned above, profiles of mass mixing ratios cannot directly be compared to ‘ceilometer profiles’. The latter can be expressed as particle backscatter coefficient $\beta_p(z)$ or as attenuated backscatter $\beta^*(z)$

$$\beta^*(z) = \beta(z)\, \exp\left\{-2\int\limits_0^z \alpha(z')\mathrm{d}z'\right\} \tag{2}$$

with z being the height, β and α the backscatter and the extinction coefficient, respectively. From the model results $\beta^*(z)$ and $\beta_p(z)$ can be calculated straight forward and the computational effort is comparable. Retrieval of both $\beta^*(z)$ and $\beta_p(z)$ from ceilometer measurements require the calibration of the ceilometer, i.e. the determination of the lidar constant C_L (also known as calibration factor). The derivation of $\beta_p(z)$ requires furthermore an inversion of the signals (e.g. Klett, 1981; Fernald, 1984) relying on the assumption of a particle lidar ratio S_p, which is highly dependent depends on the aerosol composition.

Consequently, additional uncertainties are introduced. It can be expected that the relative error of β_p is as good as approximately 15 % for specific Lufft ceilometers (Wiegner and Geiß, 2012) but can also exceed 30%. Note that water vapor absorption must be taken into account for ceilometers operating ~~at 905~~ near 910 nm, otherwise ~~β_p can be wrong by a factor of 2~~ an additional uncertainty depending on the water vapor content and the spectrum of the emitted laser radiation is introduced (Wiegner and Gasteiger, 2015). Fortunately, this does not apply for the ceilometers of the DWD ~~, but is~~ which measure at 1064 nm. However, this effect may be relevant for other ceilometer networks.

For these reasons, and because weather services are in favor of the attenuated backscatter for intercomparisons, we chose $\beta^*(z)$ as the common quantity in this study~~for model evaluation~~. In this section, the procedures to derive attenuated backscatter from model simulations and ceilometer measurements are presented in detail.

3.1 Attenuated backscatter from model output

The model outputs consist of the mass mixing ratios $m_{p,i}$ of the 11 aerosol types and no optical property of aerosol is provided. Therefore, we have to convert the model output to attenuated backscatter to compare to ceilometer measurements. In a first step the mass mixing ratios of each aerosol type are converted to mass concentrations $c_{p,i}$ by multiplying with the air density ϱ_{air} as shown in Eq. (3), with the air density calculated from the temperature and pressure profiles of the IFS-model.

$$c_{p,i}(z) = \varrho_{\mathrm{air}}(z)\, m_{p,i}(z) \qquad \text{for i=1,2,...,11} \tag{3}$$

The particle extinction coefficient $\alpha_{p,i}$ of each aerosol type i is calculated using fundamental relations of scattering theory as shown in Eq. (4).

$$\alpha_{p,i}(z) = \pi \int_{r_1}^{r_2} r^2\, Q_{\mathrm{ext,i}}(z)\, \frac{dN_i(r)}{dr}\, dr \tag{4}$$

where $Q_{\mathrm{ext,i}}$ is the extinction efficiency, and r_1 and r_2 the lower and upper limits of the size bin. The particle backscatter coefficient is defined in a similar way:

$$\beta_{p,i}(z) = \pi \int_{r_1}^{r_2} r^2\, Q_{\mathrm{bsc,i}}(z)\, \frac{dN_i(r)}{dr}\, dr \tag{5}$$

with $Q_{\mathrm{bsc,i}}$ being the scattering efficiency multiplied with the phase function at 180° . For convenience it is common to use the lidar ratio $S_{p,i}$

$$S_{p,i}(z) = \frac{\alpha_{p,i}(z)}{\beta_{p,i}(z)} \tag{6}$$

to calculate particle backscatter coefficients from extinction coefficients.

The extinction efficiencies and lidar ratios of each aerosol type are calculated applying the size distribution $dN(r)/dr$ and the refractive index n of the particles~~as assumed in the model~~, and by means of an appropriate scattering theory: for spherical particles the Mie theory is applied, for ~~non-spherical~~ nonspherical particles a suite of approaches is available with the T-matrix (Mishchenko and Travis, 1998) being the most frequently used option. ~~To be consistent with the current implementation of the aerosols in IFS we however rely on the Mie theory and~~ As reference, we use the Lorenz-Mie scattering algorithm (Mishchenko et al., 1999) even for ~~non-spherical~~ nonspherical aerosol types as dust, but include a detailed discussion of the influence of particle shape on lidar related optical properties in section 4.1.2. In order to retrieve the optical properties of the 11 aerosol types integration was performed according to the given size bins, otherwise the upper limit was set to $r = 20\,\mu$m. In case of hygroscopic growth of particles, their physical size, refractive index and density change according to the look up table mentioned above.

The conversion from the mass concentration to the extinction coefficient can now readily be achieved by ~~the factor~~ using the mass extinction coefficient $\eta_{\alpha,i}$ (given e.g. in m^2/g)

$$\eta_{\alpha,i} = \frac{\alpha_{p,i}}{c_{p,i}} = \frac{3\int_{r_1}^{r_2} r^2\, Q_{\mathrm{ext,i}}\,(dN_i(r)/dr)\,dr}{4\,\varrho_p \int_{r_1}^{r_2} r^3\,(dN_i(r)/dr)\,dr} \tag{7}$$

in the radius interval of the corresponding size bin from r_1 to r_2. Finally, the extinction and backscatter coefficients of each aerosol type are determined – with consideration of Eq. (6) – according to

$$\begin{aligned} \alpha_{p,i} &= c_{p,i}\,\eta_{\alpha,i} \\ \beta_{p,i} &= c_{p,i}\left(\frac{\eta_{\alpha,i}}{S_{p,i}}\right) = c_{p,i}\,\eta_{\beta,i} \end{aligned} \tag{8}$$

Here, $\eta_{\beta,i}$ is the factor converting mass concentration to backscatter coefficient (of aerosol type i). The contribution of the air molecules is determined from the Rayleigh theory. We use the following approximation for the extinction coefficient α_m (in km^{-1})

$$\alpha_m(z,\lambda) = 8.022\cdot 10^{-4}\varrho_{\mathrm{air}}(z)\,\lambda^{-4.08}$$

with the air density given in kg/m^3 and the wavelength λ in μm. The ~~profile of ϱ_{air} can be taken from the IFS output. The~~ molecular lidar ratio S_m is known to be

$$S_m = \frac{\alpha_m}{\beta_m} \approx \frac{8\pi}{3}$$

~~For calculating $\beta^*(z)$, Eq. (2)~~Finally, we have to take all contributions into account, i.e., the (total) extinction coefficient α is determined according to

$$\alpha = \alpha_m + \sum_{i=1}^{11} \alpha_{p,i} + \alpha_w \tag{9}$$

and the (total) backscatter coefficient is

$$\beta = \beta_m + \sum_{i=1}^{11} \beta_{p,i} \tag{10}$$

Ultimately, the attenuated backscatter $\beta^*(z)$ can be calculated as described in Eq. (2). Note, that the effective water vapor absorption coefficient α_w must only be considered in Eq. (9) if model results shall be compared to ceilometers operating in the spectral range around ~~905~~ 910 nm (Wiegner and Gasteiger, 2015). This is e.g. the case if Vaisala-ceilometers ~~are~~ were applied.

To increase the efficiency of the computations, $\eta_{\alpha,i}$ and $S_{p,i}$ are pre-calculated. An overview of aerosols in dry conditions for ~~five different wavelengths~~ the ceilometer wavelength (1064 nm) is given in Table 1. The wavelengths ~~correspond~~ corresponding to Nd:YAG-lasers used for aerosol remote sensing (355 nm, 532 nm and 1064 nm), the widely used Vaisala ceilometers (910 nm), and the 'typical wavelength' for radiative transfer calculations in the shortwave spectral range (550 nm) are also shown in Table A1 in the appendix. Note, that the lidar ratios of some aerosol types differ from values published by, e.g., Groß et al. (2015) because of the limits of the particle size bins.

Table 2. ~~Microphysical properties~~ Ceilometer sites within a distance of ~~dry aerosols assumed~~ 20 km to the nearest IFS model grid point, altitude is given in meters above mean sea level, the distance to the nearest model grid point (in km) is given in the 5. column.

No.	Site	Latitude (°N)	Longitude (°E)	Altitude (m)	Distance (km)
1	Geisenheim	49.9866	7.9551	110	3.8
2	Wunsiedel	50.0316	11.9745	622	4.0
3	Elpersbüttel	54.0692	9.0105	3	7.8
4	Friesoythe	53.0500	7.9000	6	8.7
5	Boltenhagen	54.0027	11.1909	15	12.5
6	Pelzerhaken	54.0893	10.8773	1	12.7
7	Alfeld	51.9644	9.8072	144	14.1
8	Soltau	52.9605	9.7930	76	14.2
9	Bamberg	49.8743	10.9206	240	14.5
10	Gera	50.8813	12.1289	311	16.2
11	Görlitz	51.1633	14.9531	240	18.0
12	Offenbach	50.0894	8.7864	121	18.1

3.2 Attenuated backscatter from ceilometers

Attenuated backscatter β^* can be derived from the background corrected ceilometer signals P if the system has been calibrated, i.e., if ~~the lidar constant~~ C_L ~~has been determined~~is known.

$$\beta^*(z) = \frac{Pz^2}{C_L} \tag{11}$$

It should be emphasized that C_L can vary with time (e.g. caused by aging of components, or temperature drifts)~~. However, such changes are typically slow~~, thus calibration should be performed on a regular basis whenever weather conditions permit.

The calibration of the ceilometers of the network is performed routinely by the DWD in a fully automated procedure. It is based on the TOPROF/E-Profile Rayleigh calibration routine provide by MeteoSwiss. The calibration relies on the Rayleigh method (Barrett and Ben-Dov, 1967). This is feasible under clear sky conditions and stable aerosol distributions, thus, the applicability depends on the measurement site. In order to avoid adverse influences caused by background sun light, only night time data are used for the calibration. The calibration is based on data averaged over 1 - 3 hours, and only one period is selected per night. Meteorological data used for the Rayleigh calibration are taken from the joint product of the National Centers for Environmental Prediction (NCEP) and the National Center for Atmospheric Research (NCAR) reanalysis data (Kalnay et al., 1996). The derived ~~lidar constants~~ C_L are first cleaned for outliers and then smoothed with a 30 days running mean. ~~Lidar~~ Calibration constants outside 1.5 times of the 25 to 75 percentile range of a 30 days-period are considered as outliers. The smoothed C_L are finally interpolated to hourly values to be used in Eq. 11. The ~~calibration routine implemented in the DWD automatic calibration is based on the ToProf E-Profile Rayleigh calibration routine provide by MeteoSwiss~~typical uncertainty of an individual calibration is 15 - 20 %, while the actual error is smaller due to the temporal smoothing. The accuracy of the retrieved β^* linearly depends on the accuracy of the C_L. The monthly variation of C_L is usually less than 5 % and the annual variation is 10 - 15 %. Then, attenuated backscatter β^* profiles are derived in steps of three hours, by averaging cloud free data within 30 minutes each before and after the corresponding model time. Longer averages are desirable in view of a better signal to noise ratio but are critical during day time ~~when~~ if the aerosol distribution is rapidly changing in time. In cases of rain, ~~snowfall, fog~~fog, snowfall and low level clouds (below 2 km), the data are excluded from the evaluation. The ~~corresponding information is taken from the~~ data quality flag ‘sky-condition-index’ ~~and ‘cloud-base-height’ provided by~~ from the proprietary software of the ceilometer ~~.~~

~~The accuracy of the retrieved β^* linearly depends on the accuracy of the calibration constant C_L which can be quite different for different sites and instruments~~labels corresponding measurements and cases of reduced window transmission due to droplets on the window. The altitude of the cloud bottom is determined by a complex algorithm based on signal slopes and thresholds; the details are not disclosed to the user.

4 Results and discussions

There are many several options to discuss the agreement of β^*-profiles from model calculations and ceilometer measurements: criteria include the comparison of absolute values of β^*, the general 'shape' of the profiles, the vertical extent of the mixing layer and elevated layers, the vertical structure of the aerosol distribution within the mixing layer, and more. A general philosophy on a ranking of different criteria has not yet been developed, e.g., there is no common agreement how to rate profiles when the modeled altitude of an elevated layer is consistent with measurements but the absolute values of β^* are (quite) different. The reason is that the attenuated backscatter of e.g. an elevated Saharan dust or volcanic ash layers may disagree even in the case of the same β_p because β^* does not only depend on the aerosol properties of that layer, but is also influenced by the extinction below that layer. In order to minimize this influence and to consider that part of the atmosphere where most of the aerosols typically reside, we focus in this paper on β^* of the lowermost part of the troposphere excluding the range of incomplete overlap. All ceilometer data have undergone an individual overlap correction provided by the manufacturer that makes it possible to use profiles for aerosol remote sensing from above approximately 200 m. In the following, we compare β^* averaged from the typical height of a 'reliable overlap correction' (set to 200 m for all instruments) to 1 km above ground, henceforward referred to as 'near surface average' $\overline{\beta^*_{ns}}$. An additional approach of comparison is discussed in Sect. 4.2.

Our investigation is based on measurements from 1. 1 September 2015 until 31. 31 August 2016. Attenuated backscatter profiles are derived from the model results for every 3 hours following the procedure outlined in section 3.1. Ceilometer data are averaged over 1 hour around the model time and only profiles are considered that reach at least a height of 2 km above the ground, i.e., profiles contaminated by profiles with low level clouds and precipitation are excluded from the analysis. As a consequence, averages consider 240 ceilometer profiles at maximum.

4.1 Comparison of near surface attenuated backscatter

For an overview the complete time series of the model simulation and ceilometer observation of the near surface attenuated backscatter $\overline{\beta^*_{ns}}$ over Elpersbüttel is shown in Fig. 3. This site has been chosen as it is one of the closest to the corresponding model grid point (only 7.8 km south west of the ceilometer site, see Table 2) and the orography around the measurement site is quite flat. For Elpersbüttel we found 1305 cases out of 2920 (365 × 8) when intercomparisons could take place. The number of cases varies in a range from 900 (Wunsiedel) to 1763 (Boltenhagen). Results show that the model and ceilometer data both show a similar temporal development with larger $\overline{\beta^*_{ns}}$ during winter and spring. Note, that due to cloudy weather during winter the number of useful ceilometer measurements is reduced compared to summer. In cases of low aerosol load there is a general agreement of both data sets. However, when episodes of large values of $\overline{\beta^*_{ns}}$ are modeled they typically exceed the observed ones by a factor of two or more. This is e.g. the case in December 2015, beginning of February 2016 and April 2016. 2016, more detailed investigations are presented in Section 4.1.2 and Section 4.2. The reasons for this overestimate must remain speculative - maybe it is due to erroneous assumptions of the aerosol emission or meteorological data. On the other hand the annual mean derived from the model $\overline{\beta^*_{ns}} = 1.35 \times 10^{-3}\,\mathrm{km}^{-1}\,\mathrm{sr}^{-1}$ agrees very well with the corresponding value of $\overline{\beta^*_{ns}} = 1.31 \times 10^{-3}\,\mathrm{km}^{-1}\,\mathrm{sr}^{-1}$ from the ceilometer observations at Elpersbüttel. Table 3 summarized the annual mean $\overline{\beta^*_{ns}}$

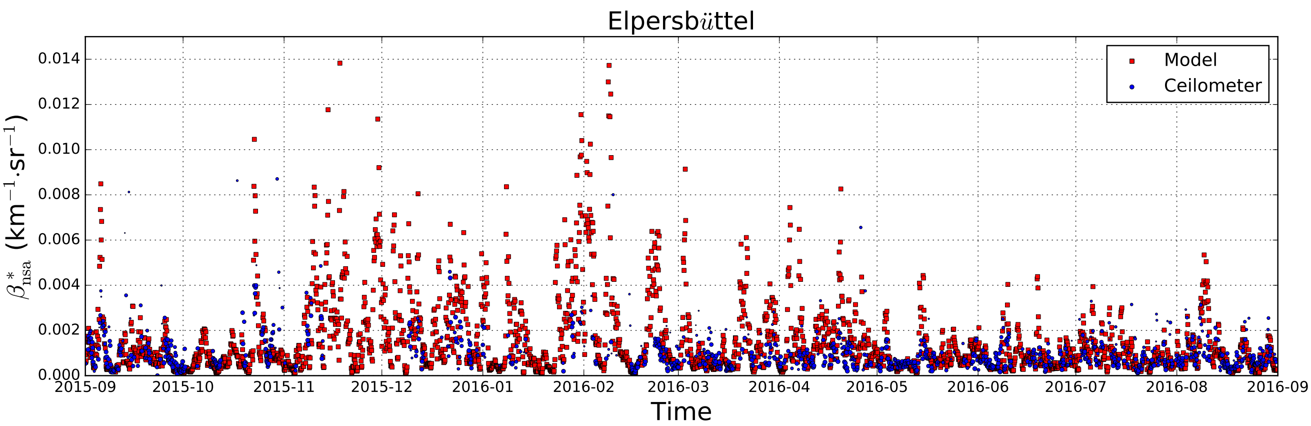

Figure 3. Time series (from 1 September 2015 to 31 August 2016) of the model simulation and ceilometer observation of near surface attenuated backscatter $\overline{\beta^*_{ns}}$ in km^{-1} sr^{-1} over Elpersbüttel with $\overline{\beta^*_{ns}}$ being averaged from 200 m ("full overlap height") up to 1 km above ground.

of both ceilometer measurements and model simulations from all 12 measurement sites. For most of the other siteslisted in Table 2sites, the model obtains higher values than the ceilometer measurements by ∼20 % on annual average. This is still a considerably good agreement. Few exceptions are Bamberg, Boltenhagen and Gera where the model predicts much lower values than observed. The largest difference of a factor of 1.8 is found for Gera with measurement and model mean values of $\overline{\beta^*_{ns}} = 1.85 \times 10^{-3}$ km^{-1} sr^{-1} and $\overline{\beta^*_{ns}} =$ 9.99 1.00 $\times$ 10^{-4} $^{-3}$ km^{-1} sr^{-1}, respectively. These stations show larger impacts from the local emissions as they are situated close to the cities. The discrepancy between ceilometer observations and model predictions over these three sites is mainly due to the differences in the spatial coverage. As the model resolution is rather coarse (1° × 1°)and therefore the model resulting in an underestimation of , the model is underestimating the aerosol concentrations over cities due to the averaging effect over large grid cell.

For a more detailed analysis we have calculated the differences Δ between modelled modeled and ceilometer derived $\overline{\beta^*_{ns}}$ with

$$\Delta = \overline{\beta^*_{ns}}(\mathrm{mod}) - \overline{\beta^*_{\mathrm{ns}}}(\mathrm{obs}) \tag{12}$$

for Elpersbüttel (see Fig. 4a). The size of the markers is proportional to the number of ceilometer measurements (up to 240) available for each individual intercomparison. The standard deviation σ of the difference is $\sigma = 1.89 \times 10^{-3}$ km^{-1} sr^{-1}, i.e. quite large compared to the model mean value of $\overline{\beta^*_{ns}} = 1.35 \times 10^{-3}$ km^{-1} sr^{-1}. Data points with $\Delta > 3\sigma$ $|\Delta| > 3\,\sigma$ are considered as outliers (marked in red in Fig. 4a) and filtered out in the subsequent analysis. Remaining The remaining data are then used to recalculate the standard deviation ($\sigma = 1.20 \times 10^{-3}$ km^{-1} sr^{-1}). The recalculated standard deviation is marked on , shown as a horizontal line in Fig. 4a.

Table 3. Summary of the annual mean $\overline{\beta^*_{ns}}$ of both ceilometer measurements and model simulations from all 12 measurement sites. The standard deviation σ of the differences is also indicated.

No.	Site	annual average ceilometer $\overline{\beta^*_{ns}}$ ($\times 10^{-3}\,\mathrm{km}^{-1}\,\mathrm{sr}^{-1}$)	annual average model $\overline{\beta^*_{ns}}$ ($\times 10^{-3}\,\mathrm{km}^{-1}\,\mathrm{sr}^{-1}$)	standard deviation of difference σ ($\times 10^{-3}\,\mathrm{km}^{-1}\,\mathrm{sr}^{-1}$)
1	Geisenheim	0.91	1.12	1.25
2	Wunsiedel	1.05	0.82	0.90
3	Elpersbüttel	1.31	1.35	1.20
4	Friesoythe	1.31	1.20	1.58
5	Boltenhagen	1.87	1.28	1.46
6	Pelzerhaken	1.13	1.24	1.13
7	Alfeld	1.07	1.13	1.31
8	Soltau	1.17	1.14	1.31
9	Bamberg	1.39	0.94	1.88
10	Gera	1.85	1.00	1.97
11	Görlitz	0.94	0.82	0.71
12	Offenbach	0.80	0.90	0.78

To better understand possible reasons for these differences we have looked into the contribution of different aerosol types. Their relative contributions to $\overline{\beta^*_{ns}}$ as calculated from the model for Elpersbüttel reveal that sea salt is by far the dominating contributor with 61 % (annual mean). Sulfate contributes with 29 % to the near surface attenuated backscatter, while organic matter (4 %), dust (3 %) and black carbon (2 %) only show minor contributions. We have re-calculated these contributions separately for two classes: cases of ‘good’ agreement (~~$\Delta<\sigma$~~$|\Delta|<\sigma$) are shown in Fig. 4b, whereas cases of ‘bad’ agreement (~~$\Delta>\sigma$~~$|\Delta|>\sigma$) are shown in Fig. 4c. Each aerosol type is color coded as indicated in the legend.

From Fig. 4b it is immediately visible that for the good agreement sea salt is again the dominating aerosol type: its contribution ranges between 32 % (May 2016) and 85 % (December 2015) with an annual average of 51 %. The second important contributor are sulfate aerosols (32 % on average) whereas all other types are in the range of a few percent each. Thus, cases of good agreement coincide with a sea salt contribution lower than the mean. Consequently, the contribution of sea salt is above the average when the differences between model and measurement are large (~~$\Delta>\sigma$~~$|\Delta|>\sigma$). From Fig. 4c a mean relative contribution of sea salt of 74 % for the ‘bad’ agreement is ~~derived~~found. This suggests that the ceilometer and model discrepancy increases with increasing sea salt contribution.

Scatter plots of the ceilometer and the model derived near surface attenuated backscatter for the 12 sites are shown in Fig. 5. The color code represents the relative contribution of sea salt to $\overline{\beta^*_{ns}}$. For most sites red dots are predominant, indicating the high contribution of sea salt. This phenomenon has already been discussed in case of Elpersbüttel. When the sea salt contribution is rather low, the model typically shows lower $\overline{\beta^*_{ns}}$ than the ceilometer retrieval. This is probably due to local emissions which

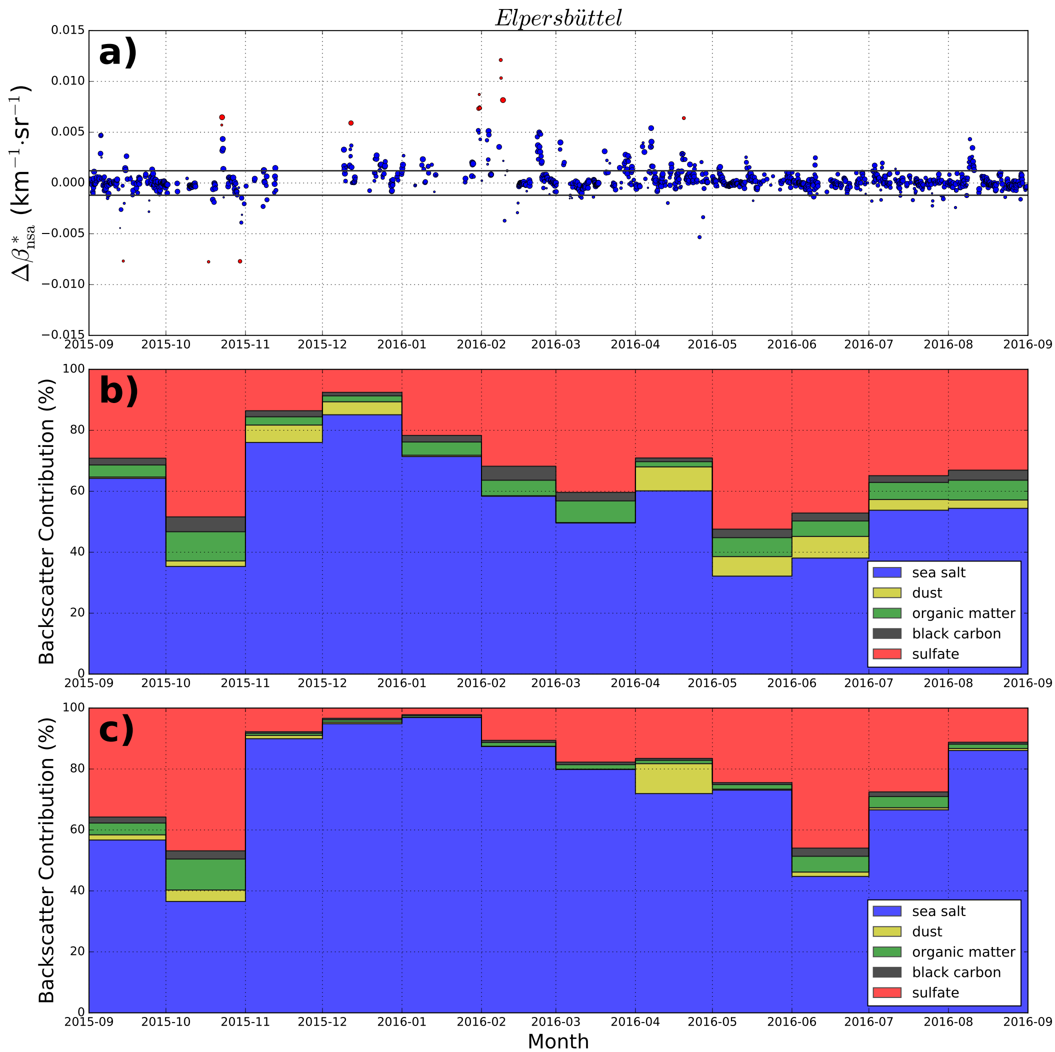

Figure 4. (a) Differences Δ of near surface attenuated backscatter $\overline{\beta^*_{ns}}$ for Elpersbüttel according to Eq. 12. The horizontal line indicates the standard deviation σ of the differences. The size of the markers represents the number of ceilometer measurements available for each individual comparison. Differences $|\Delta| > 3\,\sigma$ are shown in red. (b) Contribution of different aerosol types to $\overline{\beta^*_{ns}}$ for cases with $|\Delta| < \sigma$. (c) same as (b) but cases with $|\Delta| > \sigma$.

are not well resolved by the model but captured by the ceilometer measurements. The total least squares regression line is based only on intercomparisons when the hourly averaged data contains at least 120 ceilometer profiles could be evaluated(30 minutes of measurements). The regression is virtually unchanged when the number of valid ceilometer profiles is used as a weight. The slope of the regression line is larger than 1 for all sites, indicating that the model in general results in larger $\overline{\beta^*_{ns}}$. In particular this is true when the modeled contribution of sea salt is high, e.g. for Friesoythe, Geisenheim and Offenbach.

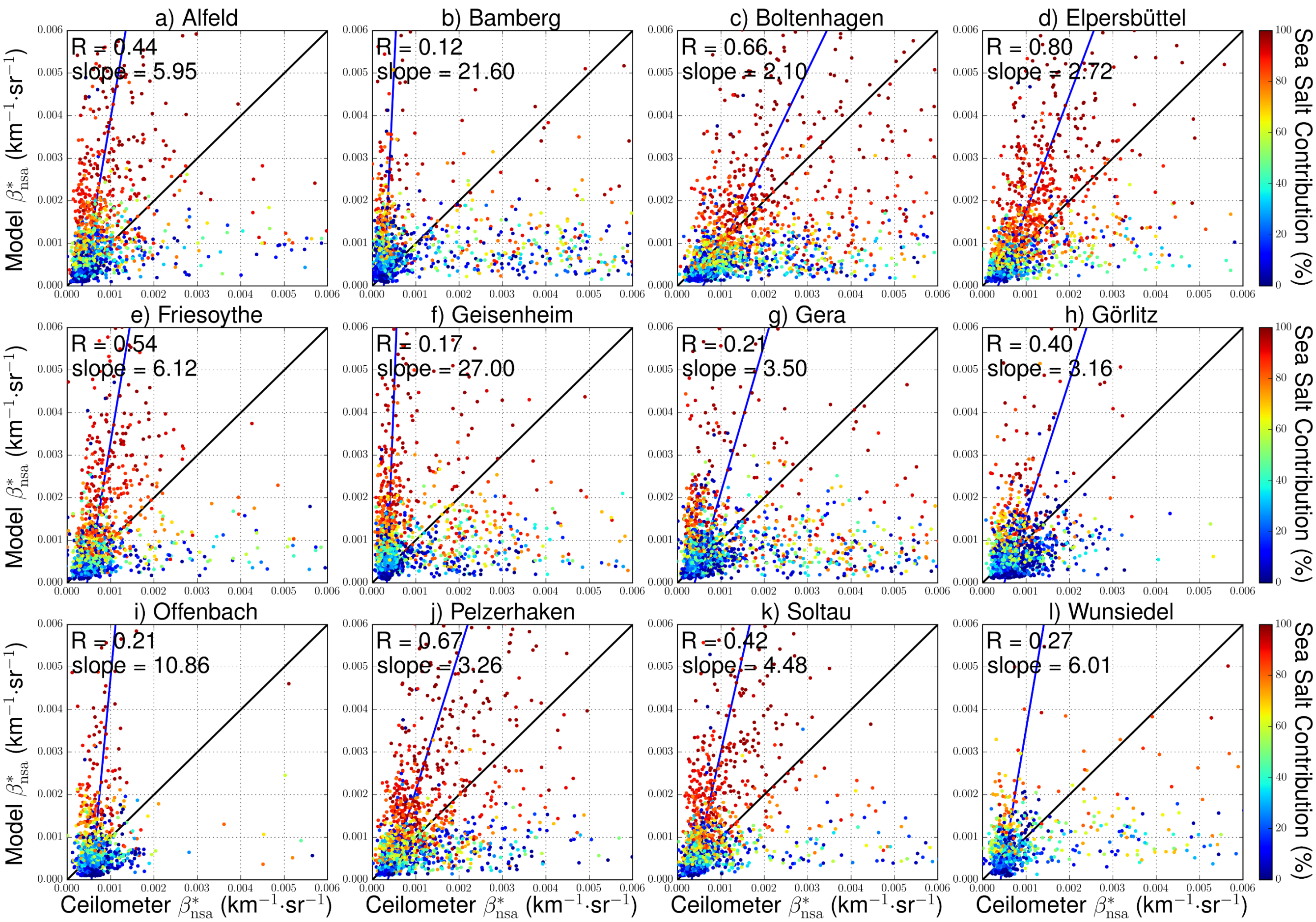

Figure 5. Scatter plots of ceilometer derived and modeled $\overline{\beta^*_{ns}}$ for the 12 sites listed in Table 2. The color code represents the relative contribution of sea salt to $\overline{\beta^*_{ns}}$. The blue curve indicates the total least squares regression line of the data points with at least 120 ceilometer profiles, while the black line represents the 1 to 1 reference.

Note, that the latter two stations are far from the coast so that the large sea salt contribution seems to be unrealistic. Pearson's correlation coefficient R ranges between $R = 0.12$ for Bamberg and $R = 0.80$ for Elpersbüttel with no clear dependence on the distance between the model grid point and the ceilometer site.

Reasons for the disagreement can be manifold: One possibility is that the backscatter per unit mass of sea salt is too large in the model. As the optical properties of sea salt critically depend on the hygroscopic growth we have investigated to which extent this effect might explain the observed differences (see section 4.1.1). Another reason could be that the modeled sea salt concentration is generally overestimated, and that it should partly be replaced by an aerosol type that is less effectively backscattering. A though the annual averaged contribution to the total aerosol optical depth (AOD) is ranging from 21 %

(Görlitz) to 37 % (Elpersbüttel), which is in a reasonable range. One the other hand this is much less than the contribution to $\overline{\beta^*_{ns}}$ demonstrating that sea salt is quite effectively backscattering, suggesting that it might partly be substituted by a less effective species to get a better agreement. A further discussion of this topic is however beyond the scope of this paper.

4.1.1 Influence of hygroscopic growth

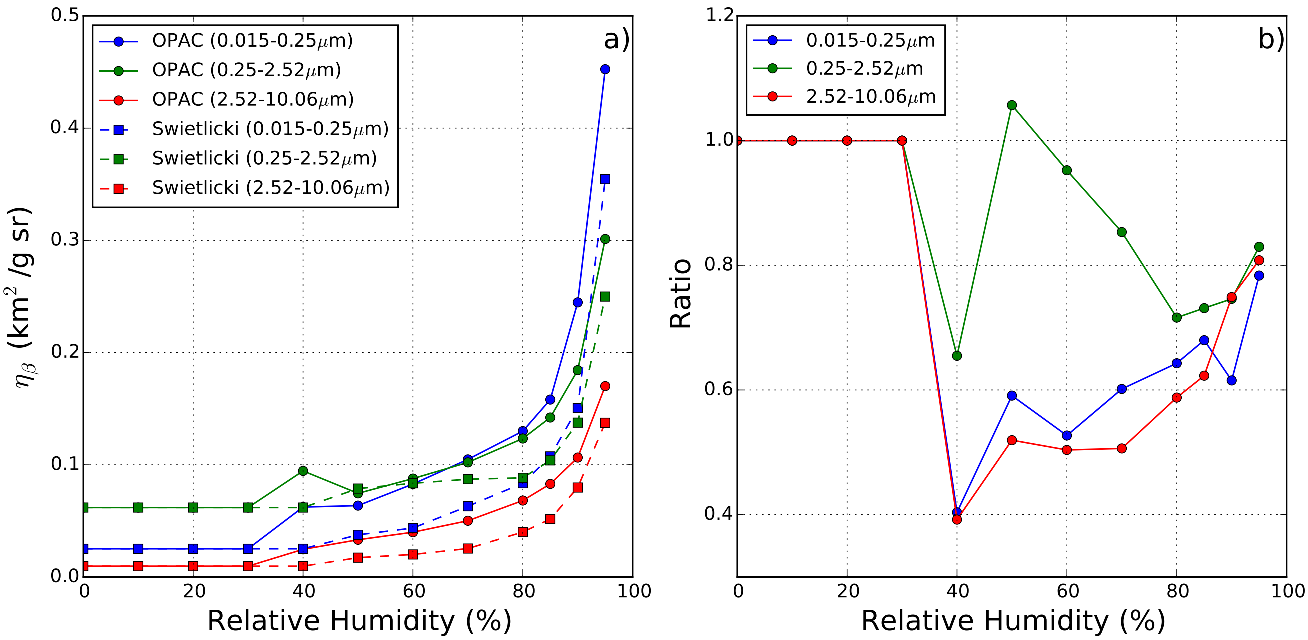

Figure 6. a) Mass mixing ratio to backscatter coefficient conversion factors $\eta_{\beta,i}$ of sea salt aerosol for the three small, medium and large size bin (in blue, green and red) at different ambient relative humidities. Hygroscopic growth factors of sea salt are taken from the model assumption (solid circle curve) and Swietlicki et al. (2008) (dashed square curve). The ratio of mass mixing ratio to backscatter coefficient conversion factors between the hygroscopic growth effects taken from Swietlicki et al. (2008) and OPAC databases are shown in b), ratios smaller than 1 indicate an reduction when using hygroscopic growth from Swietlicki et al. (2008).

Water uptake by particles has a significant impact on their optical properties as particles can change in size, chemical composition and refractive index depending on the ambient relative humidity. The assumptions made for their hygroscopic growth have a significant effect on the simulation of ceilometer measurements from the model output. For this reason, we examine the hygroscopic growth effect on the conversion factor η_β for sea salt (see Eq. 8) as the dominating aerosol species (in terms of backscatter) according to the IFS output. We compare two approaches, being aware that more are existing (e.g., Chin et al., 2002): the ~~growth model used~~ particle hygroscopic growth model implemented in the IFS ~~model~~ AOD calculation (based on OPAC, Hess et al. (1998)) and a more recent approach (Swietlicki et al., 2008), see Fig. 1. The latter was reported to better match experimental data (Zieger et al., 2013). Compared to OPAC it shows a less pronounced particle growth with relative humidity. The corresponding conversion factors $\eta_{\beta,ss}$ of sea salt are shown in Fig. 6a for comparison. Results referring to the three different size bins of the particle model are shown in blue, green and red, respectively. The ratios of the conversion factors from the two approximations ($\eta_{\beta,ss}^{(swie)}/\eta_{\beta,ss}^{(opac)}$) are shown in Fig. 6b. The conversion factors based on Swietlicki et al. (2008) are on average smaller than those based on the OPAC database, however, differently for each size bin and depending on the relative humidity. By comparing data calculated with the OPAC database, the alternative set of conversion factors $\eta_{\beta,ss}^{(swie)}$ typically on average reduce backscatter coefficients by a factor between 0.6 and 0.8, with an average of 0.78. Consequently, the change of $\overline{\beta_{ns}^{*}}$ when replacing the hygroscopic growth function can be significant and quite variable. Taking into account that sea salt particles in general contribute more than 50 % to the attenuated backscatter over Germany, overestimating the conversion factor by 22 % on average would already contribute up to an error of more than 10 % of the total backscatter signal. It should be emphasized that – as a side effect – an overestimated hygroscopic growth of sea salt leads to an increased aerosol extinction coefficient in the mixing layer. Consequently attenuated backscatter is reduced at higher altitudes, making the identification of elevated aerosol layers in principle more difficult.

In order to quantify the effect of a changed hygroscopic growth we recalculate β^* from modeled mixing ratios by using the alternative set of conversion factors (Swietlicki et al., 2008) and compare it to ceilometer observations. Analogously to Fig. 5 scatter plots of the ceilometer derived and modeled $\overline{\beta_{ns}^{*}}$ for the 12 sites are shown in Fig. 7. Compared to the original model assumptions, modeled attenuated backscatter shows a slightly better agreement with the ceilometer measurements. Although the correlation coefficients between ceilometer and model $\overline{\beta_{ns}^{*}}$ are nearly unchanged, the slope of the regression lines is on average reduced by ∼30 % and agrees better with the 1 to 1 reference line. This effect is more obvious for sites dominated by sea salt aerosols in Northern Germany, e.g. Boltenhagen, Elpersbüttel, Pelzerhaken and Soltau, while sites with lower sea salt contributions are nearly unaffected, e.g., Görlitz and Wunsiedel. The result indicates that the updated hygroscopic growth function leads to a better agreement between model simulations and measurements. However, the model is still overestimating $\overline{\beta_{ns}^{*}}$, indicating that the assumption of a reduced hygroscopic growth alone cannot fully explain the mismatch between model and observations.

4.1.2 Influence of particle shape

Besides of the hygroscopic growth of hydrophilic aerosols, the shape of particles also plays an important role for the lidar related optical properties of the particles. Mineral dust particles are typically non-sphericalnonspherical, however, they are often - e.g. in the IFS model - considered as spherical particles in order to simplify the computation. To quantify the influence of the shape-effect of mineral dust particlesshape, we compared modeled β_p and β^* using either the spherical or the non-spherical nonspherical assumption. In case of non-spherical nonspherical mineral dust particles, spheroids with an aspect ratio distribution measured by Kandler et al. (2009) and successfully applied in the closure experiment of optical properties of dust by Wiegner et al. (2009) in the framework of SAMUM, Kandler et al. (2009); Wiegner et al. (2011) are assumed in T-Matrix calculations (Waterman, 1971; Mishchenko and Travis, 1998). Table 4 shows the comparison of optical properties of dust particlestheir optical properties: it can be seen that non-spherical nonspherical particles have a significantly larger li-

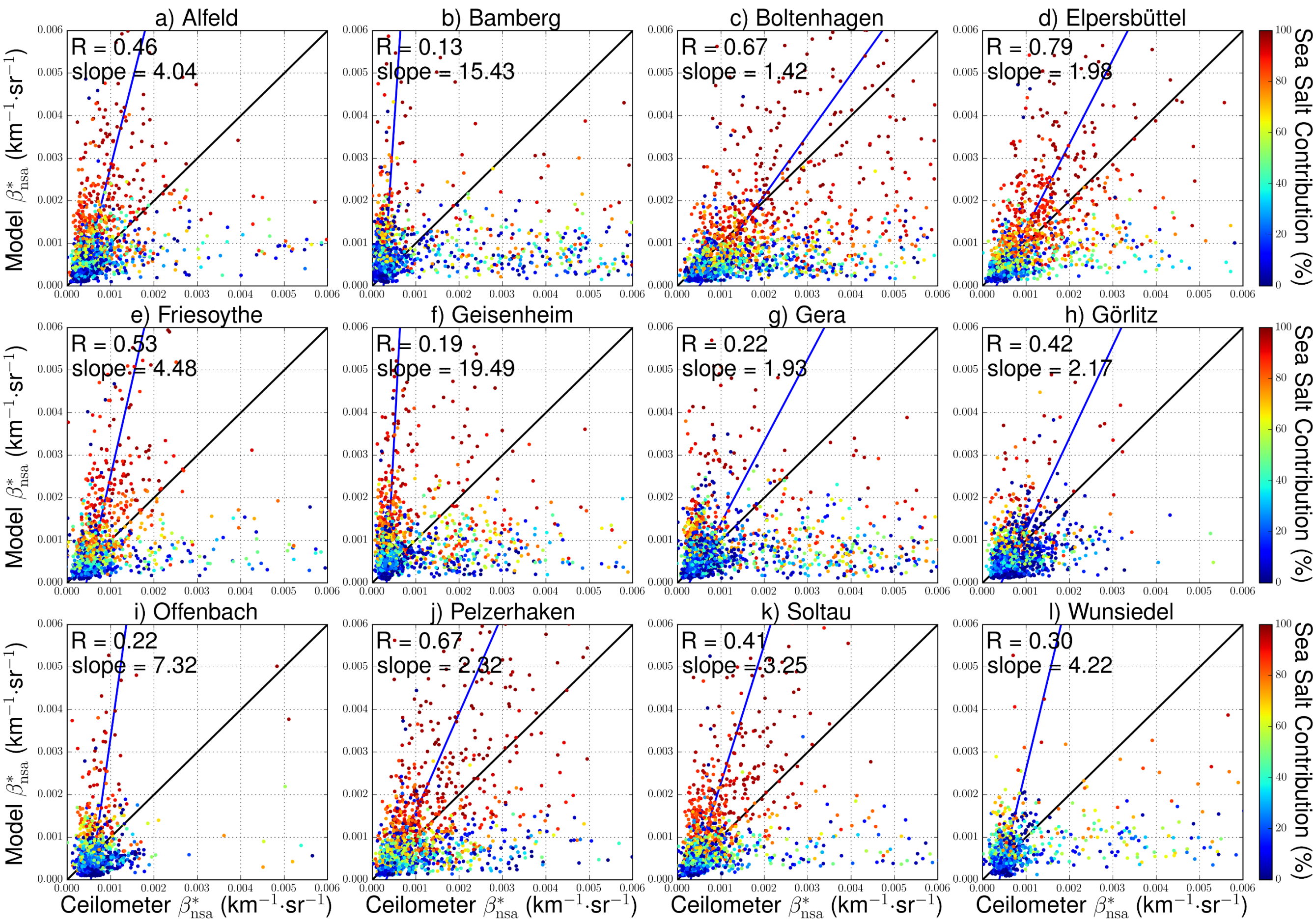

Figure 7. Scatter plots of the ceilometer and model surface attenuated backscatter signals for the 12 sites listed in Table 2. Model data are converted to attenuated backscatter signal based on hygroscopic growth factors introduced in Swietlicki et al. (2008). Color code represents the relative contribution of sea salt to backscatter signal. The blue curve indicates the total least squares regression line of data point with at least 120 ceilometer profiles, while the black curve represents the 1 to 1 reference.

dar ratio S_p whereas the specific extinction cross section σ_e^* is nearly unchanged. As a result β_p is reduced by 15 - 45 % if ~~non-sphericity~~ nonsphericity is considered, whereas the effect on the ~~extinction~~ AOD is small.

We have also investigated the influence of the treatment of particle shape on the mass to backscatter conversion factors η_β of the three dust size bins. For demonstration one 1-hour profile from a dust episode (~~3.~~ 3 April 2016, 18:00 UTC, see also next section) is discussed in detail. Attenuated backscatter profiles are shown in Fig. 8a. Ceilometer measurements with the original vertical resolution of 15 m are shown in light red, whereas the ~~bold~~ red line shows the ceilometer profile re-sampled for the model's resolution. Profiles derived from the model output for the spherical and nonspherical assumption are given in blue and green, respectively~~, for the spherical and non-spherical assumption~~. Fig. 8a clearly demonstrates that the observed decrease of

Table 4. Comparison of selected optical properties at 1064 nm of mineral dust particles assuming spherical and ~~non-spherical~~ nonspherical shapes. Spheroid particles with an aspect ratio distribution measured by Kandler et al. (2009) is assumed for ~~non-spherical~~ nonspherical dust particles.

	spherical		nonspherical		difference
species	specific extinction cross section (σ_e^*, m^2/g)	lidar ratio (S_p, sr)	specific extinction cross section (σ_e^*, m^2/g)	lidar ratio (S_p, sr)	in particle backscatter ($\Delta\ \beta_p$, %)
Dust (0.03 - 0.55 μm)	1.496	78.6	1.449	89.0	-14.4
Dust (0.55 - 0.90 μm)	1.611	48.6	1.602	69.4	-30.3
Dust (0.90 - 20.0 μm)	0.445	13.4	0.495	26.6	-44.0

β^* in the height range between ∼1.1 km and ∼3.5 km is very well reproduced by the model simulations~~, independent of the numerical treatment of the particle shape~~. However, the absolute values agree somewhat better if ~~non-sphericity~~ nonsphericity is assumed. This improvement is most pronounced in the lowermost layer where dust is the dominating contributor (see Fig. 8b and c): here the overestimate of β^* with respect to the ceilometer ~~retrievals~~ retrieval is clearly reduced but still in the order of up to a factor of 3 which also implies that the model is overestimating the dust concentration during this episode and/or the aerosol microphysical properties assumed in the forward calculation are different from the actual state. Note, that the increased attenuated backscatter at ∼8 km as observed by the ceilometer is due to the presence of clouds. The modeled β_p of the different aerosol types is shown in Fig. 8b and Fig. 8c, assuming either sphericity or ~~non-sphericity~~ nonsphericity of dust particles. Below 3 km dust is by far the dominating aerosol type. As can be expected from Table ~~4~~4, β_p of the dust component is reduced by 15 - 45 % for the three size bins when ~~non-sphericity~~ nonsphericity is considered. For the profile shown this leads to a reduction of ∼33 % of the total particle backscatter coefficient and a better agreement with the observations as ~~was~~ shown in the left panel. On the other hand, differences of the aerosol optical depth are negligible (less than 1 %) even during the dust episode. As the concentration of mineral dust aerosol is in general very low in Germany, introducing ~~non-spherical~~ nonspherical mineral dust in the IFS-model only has a minor impact on the annual average. However, in the case of dust events ~~non-sphericity~~ nonsphericity should be considered to obtain the best possible agreement. This ~~also holds~~ is also expected for volcanic ash layers which are not yet included in the model.

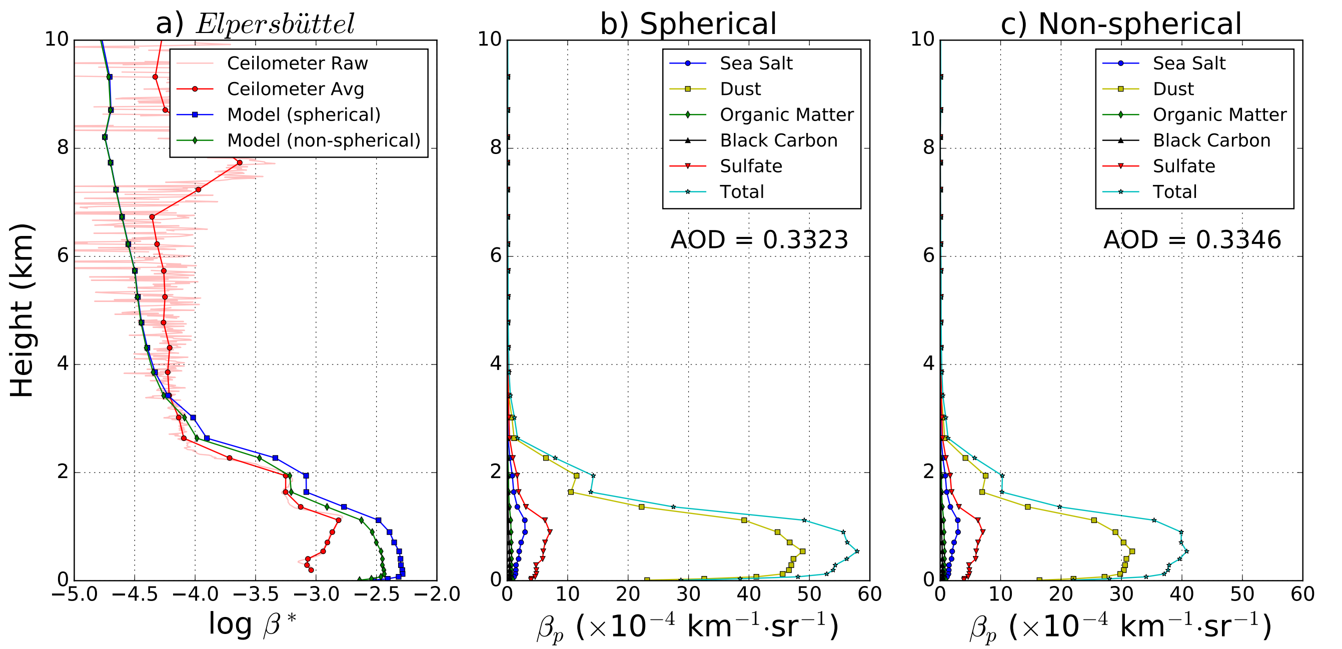

Figure 8. (a) Attenuated backscatter derived from the IFS-model and the ceilometer data, respectively, during a dust episode at 18:00 UTC on 3 April 2016 in Elpersbüttel. Model data are converted to β^* assuming either spherical (blue curve) and nonspherical (green curve) dust particles. Model results of the particle backscatter coefficient β_p (light green) together with the contributions of each aerosol type assuming either spherical (b) or nonspherical (c) particle shape. The aerosol optical depth at 1064 nm is virtually the same (AOD ≈ 0.33)

4.2 Comparison of the spatiotemporal distribution

The focus of the previous section was on the agreement of the attenuated backscatter vertically averaged over the lower troposphere. In the following case study of a dust event we briefly want to outline further options to compare model predictions and measurements of the ceilometer network.

Dust particles are typically a minor contributor to the aerosol abundance in Germany (Beuck et al., 2011; Flentje et al., 2015). On average, it contributes less than 5 % of the total attenuated backscatter according to the IFS model. However, episodes with high concentrations are observed in Germany caused by long range transport of Saharan dust towards Europe ~~(Ansmann et al., 2003; Stuut e~~ ~~From September 2015 to August 2016~~ (Ansmann et al., 2003; Stuut et al., 2009; Müller et al., 2009; Wiegner et al., 2011). During the one year covered by our study there were two major dust episodes affecting Germany as a whole: in December 2015 and April 2016. The temporal development of the latter from ~~2.~~ 2 April 2016 to ~~4.~~ 4 April 2016 is shown in Fig. 9 in terms of the modeled dust concentration (in μg/m^3), averaged over the lowermost kilometer of the troposphere: the dust layer approached Germany from southwest by ~~2.~~ 2 April and covered large parts of Germany when moving eastwards (~~3. and 4. April~~ 3 and 4

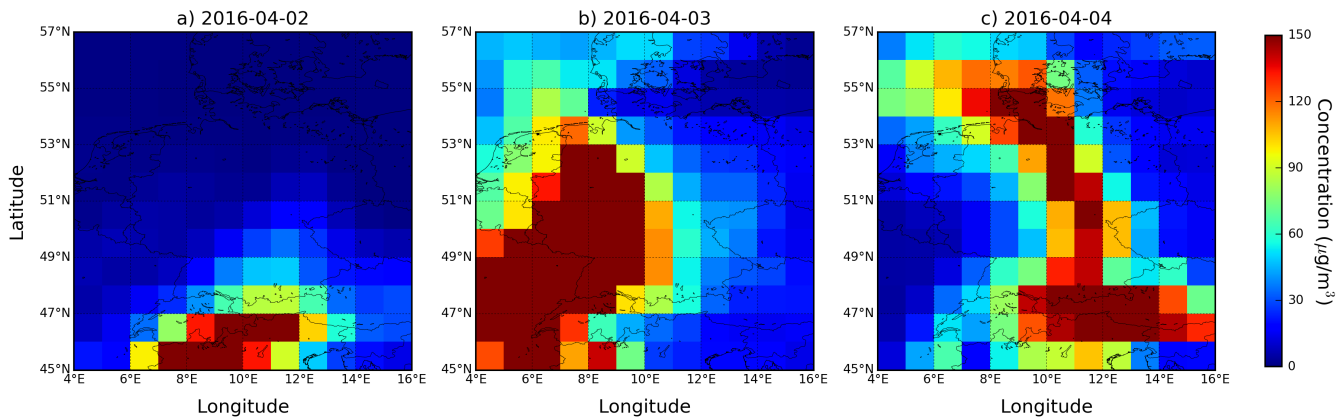

Figure 9. Dust concentration (averaged over the lowermost kilometer of the troposphere, in μg/m^3) over Germany as predicted from the IFS-model: 2 April to 4 April 2016 (from left to right), 12:00 UTC

April 2016). The episode came to an end on ~~5.~~ 5 April when only Austria was still affected~~(not shown)~~. During this event all 12 sites show peak dust contributions of over 50 % of the total $\overline{\beta^*_{ns}}$.

Again we choose Elpersbüttel as an example for the agreement between model and observations. Fig. 10a shows the time-height cross section of the attenuated backscatter of the ceilometer and in Fig. 10b the corresponding profiles calculated from the model output (blue curve) and retrieved from the ceilometer (red curve). Here we treat dust particles as ~~spheres to be consistent with the IFS-model~~nonspherical particles as defined in Section 4.1.2. Note, that due to cloud filtering some ceilometer profiles stopped at a relatively low altitude.

~~From the ceilometer measurements it seems~~ The ceilometer measurements demonstrate that the dust arrived in Elpersbüttel on 2 April 2016 at 18:00 UTC at the latest ~~;~~ (light green signatures in Fig. 10a), however, due to the presence of low level clouds the arrival could be up to 4 hours earlier. Pronounced signatures of enhanced backscatter can be observed up to almost 7 km~~(see a)~~. This is in excellent agreement with the modeled profiles for 18:00 UTC and 21:00 UTC: the aerosol layer is clearly visible up to 6 km and 7 km, respectively; even the pronounced aerosol layer up to approximately 1.5 km is resolved. The absolute values of β^* are similar with largest differences in the lowermost kilometer. For the time period before 18:00 UTC the model shows a slightly enhanced β^* at altitudes above 3 km, that is not visible in the measurements. On the other hand the vertical extent of the mixing layer is very well reproduced by the model. The enhancement of attenuated backscatter at 4 -6 km from 00:00 UTC to 06:00 UTC is due to the presence of clouds.

The temporal development of the attenuated backscatter over Elpersbüttel on ~~3.~~ the following day, 3 April 2016, is shown in Fig. 11, whereas Fig. 12 shows the contribution of particle backscatter for the five aerosol types from the model. The ceilometer measurements show an pronounced elevated aerosol layer which is clearly separated from the surface aerosol layer before 04:00 UTC. ~~It can be assumed that~~ From model simulation, the lower layer primarily contains locally produced

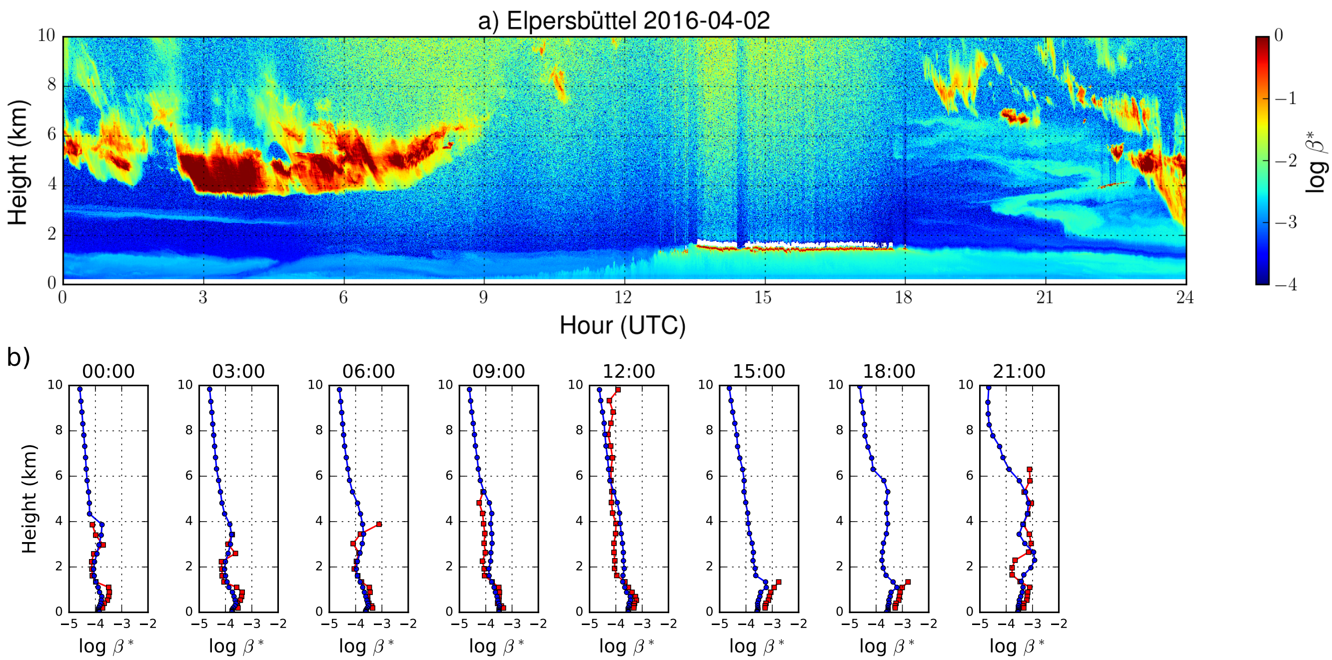

Figure 10. Time series of attenuated backscatter measured by the ceilometer at Elpersbüttel during a dust episode on 2 April 2016 is shown in (a). Attenuated backscatter calculated from model simulations (blue curve) is shown in (b), ceilometer measurements (red curve) are averaged to model resolution and shown for reference.

particles~~(typically the mixing layer height is lower than 1.5 km in spring in Germany)~~ , i.e., sulfate aerosols, whereas the upper layer is ~~Saharan~~ (Saharan) dust. This is plausible but cannot be proven from data of a single wavelength backscatter ceilometer without depolarization channel. Moreover, from the ceilometer data it is not possible to determine the top of the aerosol layer due to clouds, nevertheless measurements at 01:00 UTC and 03:00 UTC suggest that aerosols were present up to approximately 4 km for the first few hours of the night. The model shows large values of β^* up to 4 km until 09:00 UTC with dust as the dominating contributor. For the second half of the day the dust layer is confined to the lowermost 3 km according to the model (see Fig. 8). Again, the general agreement of the vertical extent of the aerosol layer is very good. However, it must remain open whether the thin layer at 6 - 7 km, visible in the modeled β^*-profiles at 09:00 UTC and 12:00 UTC is real or not. The measurement range of the ceilometer is blocked by clouds in 3 km altitude, and even under ~~cloudfree~~ cloud free conditions the ceilometer might have missed that layer due to the high solar background illumination around noon. ~~In spite of the generally good agreement of the profiles, the absolute values of β^* below 1 km sometimes differ considerably as has been already demonstrated in .~~

The situation of the last day of the event is shown in Fig. 13. From the ceilometer observations it can be ~~concluded~~ observed that the elevated aerosol layer disappears at around 19:00 UTC. ~~Prior to this, visual inspection of β^* suggest that dust is present~~

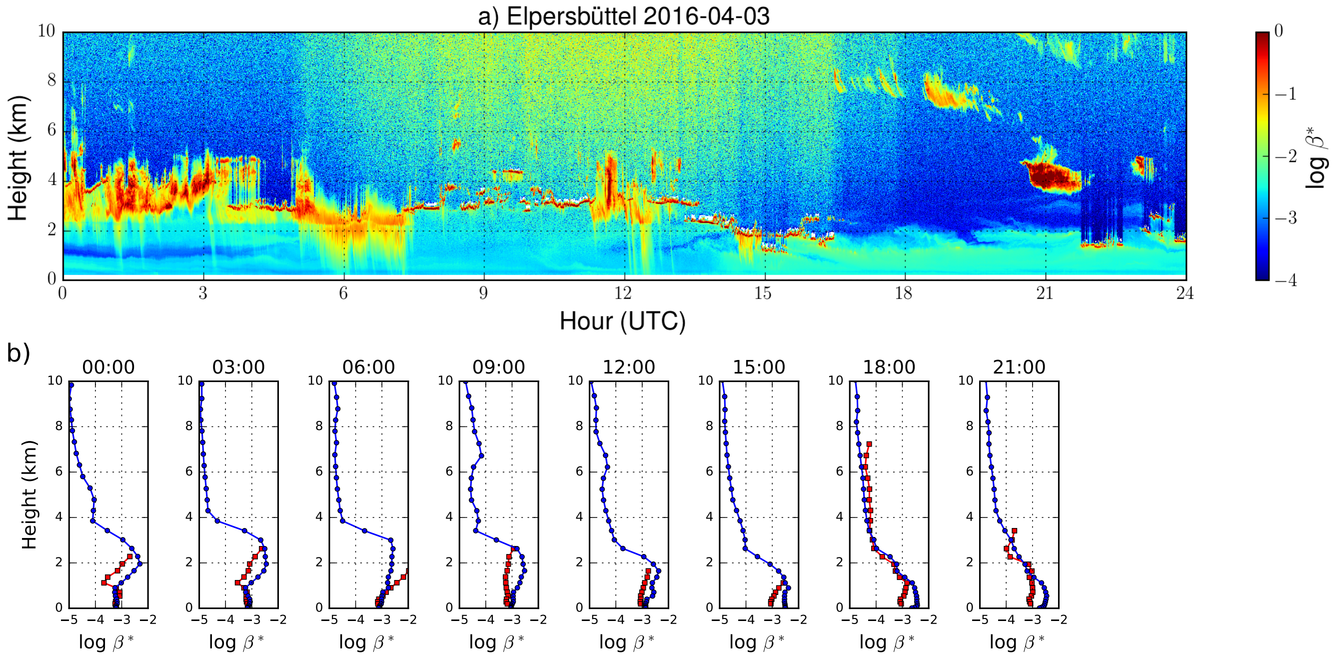

Figure 11. Same as Fig. 10 but 3 April 2016.

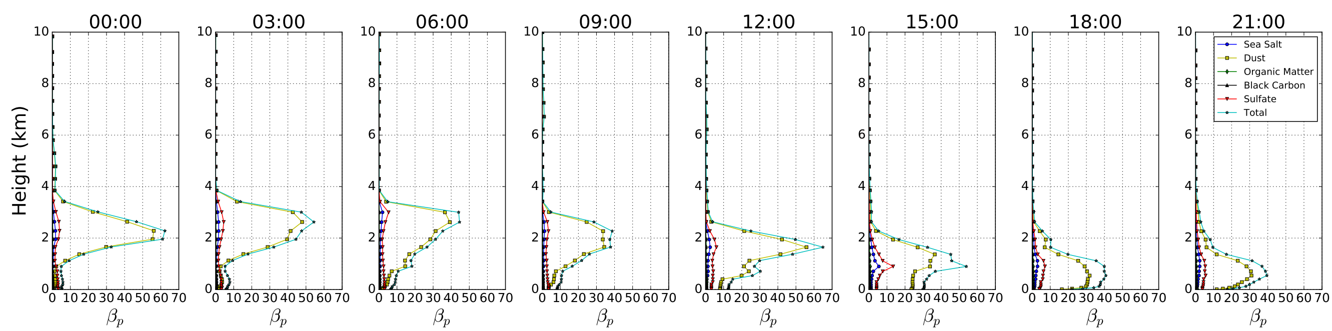

Figure 12. Time series of particle backscatter of the five aerosol types simulated by the model at Elpersbüttel during a dust episode on 3 April 2016.

~~up to at least 2 km. Again, the upper boundary cannot be detected before 08:00 UTC due to low level clouds.~~ According to the model ~~prediction~~ simulation the dust event ~~should persist~~ over Elpersbüttel ~~until~~ ended on 4 April 2016 at 18:00~~UTC or~~ - 21:00 UTC~~of 4. April 2016.~~ . This is in perfect agreement with the ~~observations~~ceilometer's attenuated backscatter profile. However, further validation of the vertical extent is hardly possible due to the above mentioned clouds. ~~It is likely that the large attenuated backscatter in the elevated layer until about 18~~Again, the upper boundary of the aerosol layer cannot be monitored

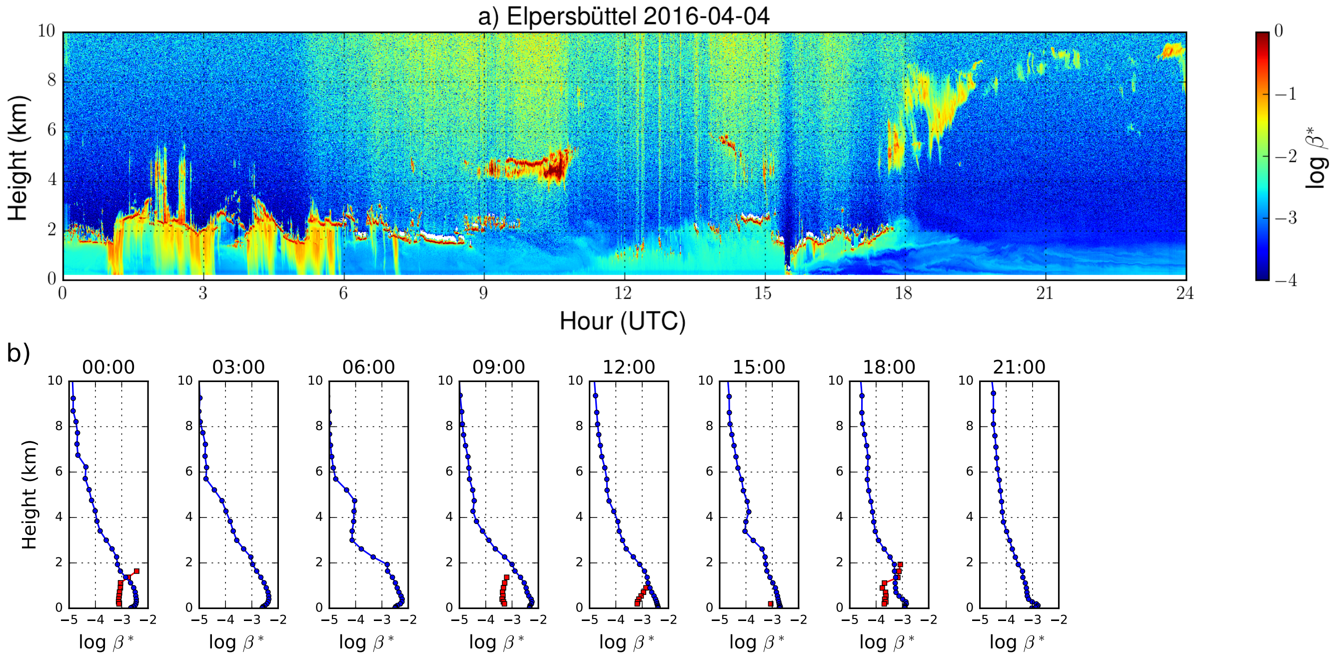

Figure 13. same as Fig. 10 but for 4 April 2016.

over the full day, e.g. before 08:00 UTC due to low level clouds. In contrast to the generally good agreement of β^* below 1 ~~-20~~km, the absolute values differ considerably on 4 April. The discrepancies could be related to the fact, that Elpersbüttel was located at the edge of the high aerosol load region at that time (see Fig. 9c). In this case, misallocation of aerosols in a single grid cell would already result in a huge error. In addition, the local aerosol distribution certainly had undergone rapid changes due to several rain showers before 07:00 UTC~~is mainly caused by dust. However, this cannot be clarified by the ceilometer measurements, as no depolarization ratios can be determined~~, that might be not resolved by the model.

The overall good agreement between model and observation is confirmed for other sites in Germany. For example, the ceilometer at Soltau, 130 km southeast of Elpersbüttel, observes the dust layer the first time on ~~2.~~ 2 April, 17:00 UTC, between 3 km and 7 km - in agreement with the model predictions. This also holds for Pelzerhaken (120 km east of Elpersbüttel) where the ceilometer measurements suggests an arrival of the layer by shortly before 22:00 UTC whereas the model results indicate a pronounced dust contribution the first time by 21:00 UTC. Another example is Alfeld, about 250 km south of Elpersbüttel, where the ceilometer observed the arrival of dust layer on 2 April, 17:00 UTC. The dust layer was then gradually descending over night and finally merged into the mixing layer on 3 April, 6:00 - 12:UTC. The time-height cross section of the attenuated backscatter of the ceilometer and the corresponding profiles calculated from the model output over Alfeld from 2. - 4 April are shown in Fig. A1, Fig. A2 and Fig. A3. In central Germany (Offenbach) the arrival time is earlier, approximately at 09:00 UTC according to both model and observations. The upper boundary of the layer is somewhat larger according to the model

(6 km vs. 4 km from the observations), however, the ceilometer measurements are subject to high solar background limiting their vertical range. For ~~3.~~ 3 April the dust event was detected at all stations. In some cases, e.g. Offenbach, the vertical extent of the layer could however not be validated due to low and mid-level clouds.

~~Taking the underlying limitations of remote sensing with a ceilometer into account we conclude that observations and model match very well : this includes the presence of the dust layer, the~~ The case study of the dust episode in April 2016 shows that the model is able to capture such a long range transport event and compare reasonably well with remote sensing measurements. A network of ceilometers is a powerful tool to validate the arrival, the temporal development and the vertical extent of the ~~layer and – to a lesser extent – also~~ dust layer as long as low clouds or precipitation do not block the signals. The agreement of the absolute values of β^* ~~. Discrepancies in the lower part of the troposphere might partly originate from local sources of particles, that are not resolved by the model. The discrimination of different aerosol types is in principle not possible with current state-of-the-art ceilometer networks, and it is not possible to penetrate optically thick clouds anyhow. Moreover, this case study suggests that an automated numerical scheme to quantitatively intercompare modeled and measured~~ ~~β^*-profiles must be very complex.~~ is however less significant.

5 Summary and Conclusions

Numerical simulations of spatio-temporal distribution of aerosols are complex due to manifold interactions between chemistry and meteorology, and the heterogeneity of emission sources. Thus, validation of model forecasts is highly desirable. In this paper, we ~~have compared attenuated backscatter (β^*) profiles calculated from~~ take advantage of a unique infrastructure: the ceilometer network operated by the German Weather Service (DWD) providing continuous range resolved aerosol information at more than 100 stations. We have compared model simulation of the European Centre for Medium-Range Weather Forecast Integrated Forecast System (ECMWF-IFS) ~~and ceilometer networkmeasurements operated by the German weather service (DWD) over one year~~ with measurements of this ceilometer network. One year of data from September 2015 to August ~~2016. The~~ 2016 were considered, and we focus on 12 sites within 20 km of a model grid point. The intercomparison is based on attenuated backscatter β^*, a quantity that can be derived from well calibrated ceilometers. As the model includes prognostic equations for the mass mixing ratio of 11 different types of aerosols~~. In terms of backscatter coefficient~~ ~~β_p, sea salt is the dominating type (more than 50 %) for virtually all sites over Germany. If ceilometers are properly calibrated, attenuated backscatter can be derived. This quantity was chosen as the common physical quantity for the intercomparison as it is independent to the assumption of a lidar ratio in the ceilometer retrieval. The~~ , β^*-profiles ~~are calculated from the mass mixing ratios of the model~~ have to be calculated according to the inherent aerosol microphysical properties. ~~Ceilometers are used for intercomparison when a model grid point could be found within 20 km. In total, 12 sites fulfill this criterion. Comparison of the attenuated backscatter averaged over~~ Our comparison focus on the lowest part of the atmosphere~~(~~~~$\overline{\beta^*_{ns}}$~~, i.e. averages $\overline{\beta^*_{ns}}$ from the mean overlap range of ~~ceilometers of~~ the ceilometers at 0.2 km to 1 km above ground~~)~~. It shows similar annual averages, however, ~~there are several cases where the modeled~~ ~~$\overline{\beta^*_{ns}}$~~ ~~exceeds the ceilometer measurements~~the standard deviation of the difference is in 8 out of 12 sites larger than the average.

To find reasons for the disagreement, we have examined the role of hygroscopic growth of particles and the role of particle shape. We have calculated β^* substituting the ~~current~~ hygroscopic growth function of sea salt particles ~~(~~based on OPAC ~~) by a more recent function (Swietlicki et al., 2008)~~by an alternative function reported by Swietlicki et al. (2008). Our calculations show that this change results in a significant reduction of particle backscatter of sea salt. As sea salt is the major contributor to the particle backscatter coefficient, the effect on the modeled attenuated backscatter is ~~significant and~~ in the order of 10 % on average. As a consequence implementing a ~~more recent~~ realistic hygroscopic growth function ~~leads to a better~~ is essential for the agreement between ceilometer measurements and model.

The importance of ~~the~~ an adequate consideration of the ~~particle shape in~~ nonspherical shape in the case of mineral dust particles ~~is~~ was investigated separately. ~~Instead of the currently used assumption of spherical particles, we apply~~ For this purpose calculations of optical properties from the Mie theory and the T-matrix method ~~for spheroids with a measured aspect ratio distribution~~assuming spheroids were compared. Application of the ~~T-matrix method~~ latter in the framework of a a case study reduces β_p of dust by 15 - 45 %~~. A case study of a dust episode for one of the 12 selected sites, Elpersbüttel, shows~~ , resulting in a better agreement between model and ceilometer measurement~~when applying optical properties of non-spherical dust particles~~. As on average the concentration of dust aerosol is very low in Germany, a significant effect on the total attenuated backscatter is however confined to dust episodes.

Finally we have investigated the ‘agreement’ between model and observations in the case of a dust event. In this context we understand ‘agreement’ as the same time period of the event (appearance, dissolution) and the same vertical extent of the dust layer. The case study shows a quite good general qualitative agreement but also highlights the inherent problems of ceilometer measurements when low clouds are present, and ~~missing information for aerosol typing. Moreover, there is a certain degree of ambiguity in the definition of~~ the ~~‘beginning’ and ‘end’ of a dust event~~lack of information on the aerosol type due to the single-wavelength concept.

~~From our study we conclude that intercomparisons of aerosol profiles derived from models and measurements should be extended in several ways:~~

~~A~~ Intercomparisons as described will certainly benefit from a better model resolution ~~is desirable so that~~ and an extension of the ceilometer network. Then, more cases can be found where the distance between a model grid point and a ceilometer site is a few kilometers only. This would strengthen the conclusions. A recent update of the IFS does indeed provide a resolution of 0.5°, and DWD is ~~continously extending the ceilometer network(120 by the end of 2017)~~continuously extending its ceilometer network. Moreover, attenuated backscatter is included in the model’s output since ~~26.~~ 26 September 2016 ~~offering new options for~~ facilitating future intercomparisons.

~~Intercomparisons should take advantage of as many profile information as possible~~Our study demonstrated that ceilometer networks could offer several options for the validation of numerical models: not only the vertical profile of β^*, but also the agreement in terms of altitude, extent, temporal development and mean particle backscatter β_p of extended/elevated aerosol layers ~~should be addressed~~(e.g. volcanic ash) can be considered. In this paper we have discussed only one dust event for demonstration purposes and found good agreement with respect to the vertical extent of the layer and its temporal development. Whether this finding is valid in general must be investigated in further studies. This effort ~~might include~~ could benefit from the development of automated algorithms for layer detectionand particle characterization. Due to their unprecedented spatial coverage ceilometer networks may constitute the observational backbone, nevertheless the combination with a small setof advanced lidar systems should be envisaged.

Investigation of the influence of meteorological fields and the chemical formalism of the modelsupplementary data set, e.g. emission schemes, on the aerosol composition and the corresponding attenuated backscatter profiles should be encouragedfrom advanced lidar systems and photometers for particle characterization, should be fostered.

Code and data availability. The source code of the ECMWF IFS model is not available for public as it is an operational model running on routine bases. The ECMWF IFS model simulation results are available to the meteorological offices of the member states of ECMWF. The raw data of the ceilometer instruments are available on request from the data originator DWD (datenservice@dwd.de). The database of aerosol optical properties used in this study is available on request from the corresponding author (ka.chan@dlr.de).

Competing interests. The authors declare that they have no conflict of interest.

Acknowledgements. We thank Maxime Hervo and his colleagues at MeteoSwiss for the provision of the ToProf TOPROF/E-Profile Rayleigh calibration routine. This work has been partially supported by the European Center for Medium Weather Forecast (ECMWF) through its main contractor Royal Netherlands Meteorological Institute (KNMI) and KNMI's subcontractor German Weather Service (DWD) in the context of the Copernicus Atmosphere Monitoring Service (CAMS). The work described in this paper was partially supported by the Marie Curie Initial Training Network of the European Seventh Framework Programme (Grant No. 607905) and the European Cooperation in Science and Technology (COST) action 'TOPROF' of the European Union's Horizon 2020 programme (Project No. ES1303). Josef Gasteiger has received funding from the European Research Council (ERC) under the European Union's Horizon 2020 research and innovation programme (Grant No. 640458, A-LIFE).

References

Ansmann, A., Bösenberg, J., Chaikovsky, A., Comerón, A., Eckhardt, S., Eixmann, R., Freudenthaler, V., Ginoux, P., Komguem, L., Linné, H., Márquez, M. n. L., Matthias, V., Mattis, I., Mitev, V., Müller, D., Music, S., Nickovic, S., Pelon, J., Sauvage, L., Sobolewsky, P., Srivastava, M. K., Stohl, A., Torres, O., Vaughan, G., Wandinger, U., and Wiegner, M.: Long-range transport of Saharan dust to northern Europe: The 11-16 October 2001 outbreak observed with EARLINET, Journal of Geophysical Research: Atmospheres, 108, https://doi.org/10.1029/2003JD003757, http://dx.doi.org/10.1029/2003JD003757, 4783, 2003.

Baklanov, A., Schlünzen, K., Suppan, P., Baldasano, J., Brunner, D., Aksoyoglu, S., Carmichael, G., Douros, J., Flemming, J., Forkel, R., Galmarini, S., Gauss, M., Grell, G., Hirtl, M., Joffre, S., Jorba, O., Kaas, E., Kaasik, M., Kallos, G., Kong, X., Korsholm, U., Kurganskiy, A., Kushta, J., Lohmann, U., Mahura, A., Manders-Groot, A., Maurizi, A., Moussiopoulos, N., Rao, S. T., Savage, N., Seigneur, C., Sokhi, R. S., Solazzo, E., Solomos, S., Sørensen, B., Tsegas, G., Vignati, E., Vogel, B., and Zhang, Y.: Online coupled regional meteorology chemistry models in Europe: current status and prospects, Atmospheric Chemistry and Physics, 14, 317–398, https://doi.org/10.5194/acp-14-317-2014, 2014.

Balzarini, A., Pirovano, G., Honzak, L., Žabkar, R., Curci, G., Forkel, R., Hirtl, M., José, R. S., Tuccella, P., and Grell, G.: WRF-Chem model sensitivity to chemical mechanisms choice in reconstructing aerosol optical properties, Atmospheric Environment, 115, 604 – 619, https://doi.org/https://doi.org/10.1016/j.atmosenv.2014.12.033, 2015.

Barrett, E. W. and Ben-Dov, O.: Application of the Lidar to Air Pollution Measurements, Journal of Applied Meteorology, 6, 500–515, https://doi.org/10.1175/1520-0450(1967)006<0500:AOTLTA>2.0.CO;2, 1967.

Bechtold, P., Kohler, M., Jung, T., Doblas-Reyes, F., Leutbecher, M., Rodwell, M. J., Vitart, F., and Balsamo, G.: Advances in simulating atmospheric variability with the ECMWF model: From synoptic to decadal time-scales, Quarterly Journal of the Royal Meteorological Society, 134, 1337–1351, https://doi.org/10.1002/qj.289, 2008.

Benedetti, A., Morcrette, J.-J., Boucher, O., Dethof, A., Engelen, R. J., Fisher, M., Flentje, H., Huneeus, N., Jones, L., Kaiser, J. W., Kinne, S., Mangold, A., Razinger, M., Simmons, A. J., and Suttie, M.: Aerosol analysis and forecast in the European Centre for Medium-Range Weather Forecasts Integrated Forecast System: 2. Data assimilation, Journal of Geophysical Research: Atmospheres, 114, https://doi.org/10.1029/2008JD011115, d13205, 2009.

Beuck, H., Quass, U., Klemm, O., and Kuhlbusch, T.: Assessment of sea salt and mineral dust contributions to PM10 in NW Germany using tracer models and positive matrix factorization, Atmospheric Environment, 45, 5813–5821, https://doi.org/https://doi.org/10.1016/j.atmosenv.2011.07.010, 2011.

Binietoglou, I., Basart, S., Alados-Arboledas, L., Amiridis, V., Argyrouli, A., Baars, H., Baldasano, J. M., Balis, D., Belegante, L., Bravo-Aranda, J. A., Burlizzi, P., Carrasco, V., Chaikovsky, A., Comerón, A., D'Amico, G., Filioglou, M., Granados-Muñoz, M. J., Guerrero-Rascado, J. L., Ilic, L., Kokkalis, P., Maurizi, A., Mona, L., Monti, F., Muñoz Porcar, C., Nicolae, D., Papayannis, A., Pappalardo, G., Pejanovic, G., Pereira, S. N., Perrone, M. R., Pietruczuk, A., Posyniak, M., Rocadenbosch, F., Rodríguez-Gómez, A., Sicard, M., Siomos, N., Szkop, A., Terradellas, E., Tsekeri, A., Vukovic, A., Wandinger, U., and Wagner, J.: A methodology for investigating dust model performance using synergistic EARLINET/AERONET dust concentration retrievals, Atmospheric Measurement Techniques, 8, 3577–3600, https://doi.org/10.5194/amt-8-3577-2015, 2015.

Boucher, O. and Anderson, T. L.: General circulation model assessment of the sensitivity of direct climate forcing by anthropogenic sulfate aerosols to aerosol size and chemistry, Journal of Geophysical Research: Atmospheres, 100, 26 117–26 134, https://doi.org/10.1029/95JD02531, 1995.

Boucher, O., Pham, M., and Venkataraman, C.: Simulation of the atmospheric sulfur cycle in the LMD GCM: Model description, model evaluation, and global and European budgets, Tech. rep., Note, 2002.

Buizza, R., Milleer, M., and Palmer, T. N.: Stochastic representation of model uncertainties in the ECMWF ensemble prediction system, Quarterly Journal of the Royal Meteorological Society, 125, 2887–2908, https://doi.org/10.1002/qj.49712556006, 1999.

Cazorla, A., Casquero-Vera, J. A., Román, R., Guerrero-Rascado, J. L., Toledano, C., Cachorro, V. E., Orza, J. A. G., Cancillo, M. L., Serrano, A., Titos, G., Pandolfi, M., Alastuey, A., Hanrieder, N., and Alados-Arboledas, L.: Near-real-time processing of a ceilometer network assisted with sun-photometer data: monitoring a dust outbreak over the Iberian Peninsula, Atmospheric Chemistry and Physics, 17, 11 861–11 876, https://doi.org/10.5194/acp-17-11861-2017, 2017.

Chaikovsky, A., Dubovik, O., Holben, B., Bril, A., Goloub, P., Tanré, D., Pappalardo, G., Wandinger, U., Chaikovskaya, L., Denisov, S., Grudo, J., Lopatin, A., Karol, Y., Lapyonok, T., Amiridis, V., Ansmann, A., Apituley, A., Allados-Arboledas, L., Binietoglou, I., Boselli, A., D'Amico, G., Freudenthaler, V., Giles, D., Granados-Muñoz, M. J., Kokkalis, P., Nicolae, D., Oshchepkov, S., Papayannis, A., Perrone, M. R., Pietruczuk, A., Rocadenbosch, F., Sicard, M., Slutsker, I., Talianu, C., De Tomasi, F., Tsekeri, A., Wagner, J., and Wang, X.: Lidar-Radiometer Inversion Code (LIRIC) for the retrieval of vertical aerosol properties from combined lidar/radiometer data: development and distribution in EARLINET, Atmospheric Measurement Techniques, 9, 1181–1205, https://doi.org/10.5194/amt-9-1181-2016, 2016.

Chan, K. L.: Biomass burning sources and their contributions to the local air quality in Hong Kong, Science of The Total Environment, 596-597, 212–221, https://doi.org/https://doi.org/10.1016/j.scitotenv.2017.04.091, 2017.

Chan, K. L. and Chan, K. L.: Aerosol optical depths and their contributing sources in Taiwan, Atmospheric Environment, 148, 364–375, https://doi.org/http://dx.doi.org/10.1016/j.atmosenv.2016.11.011, 2017.

Chin, M., Ginoux, P., Kinne, S., Torres, O., Holben, B. N., Duncan, B. N., Martin, R. V., Logan, J. A., Higurashi, A., and Nakajima, T.: Tropospheric Aerosol Optical Thickness from the GOCART Model and Comparisons with Satellite and Sun Photometer Measurements, Journal of the Atmospheric Sciences, 59, 461–483, https://doi.org/10.1175/1520-0469(2002)059<0461:TAOTFT>2.0.CO;2, 2002.

Cuevas, E., Camino, C., Benedetti, A., Basart, S., Terradellas, E., Baldasano, J. M., Morcrette, J. J., Marticorena, B., Goloub, P., Mortier, A., Berjón, A., Hernández, Y., Gil-Ojeda, M., and Schulz, M.: The MACC-II 2007-2008 reanalysis: atmospheric dust evaluation and characterization over northern Africa and the Middle East, Atmospheric Chemistry and Physics, 15, 3991–4024, https://doi.org/10.5194/acp-15-3991-2015, 2015.

Curci, G., Hogrefe, C., Bianconi, R., Im, U., Balzarini, A., Baró, R., Brunner, D., Forkel, R., Giordano, L., Hirtl, M., Honzak, L., Jiménez-Guerrero, P., Knote, C., Langer, M., Makar, P., Pirovano, G., Pérez, J., José, R. S., Syrakov, D., Tuccella, P., Werhahn, J., Wolke, R., Žabkar, R., Zhang, J., and Galmarini, S.: Uncertainties of simulated aerosol optical properties induced by assumptions on aerosol physical and chemical properties: An AQMEII-2 perspective, Atmospheric Environment, 115, 541 – 552, https://doi.org/https://doi.org/10.1016/j.atmosenv.2014.09.009, 2015.

Dentener, F., Kinne, S., Bond, T., Boucher, O., Cofala, J., Generoso, S., Ginoux, P., Gong, S., Hoelzemann, J. J., Ito, A., Marelli, L., Penner, J. E., Putaud, J.-P., Textor, C., Schulz, M., van der Werf, G. R., and Wilson, J.: Emissions of primary aerosol and precursor gases in the years 2000 and 1750 prescribed data-sets for AeroCom, Atmospheric Chemistry and Physics, 6, 4321–4344, https://doi.org/10.5194/acp-6-4321-2006, 2006.

Drusch, M., Scipal, K., de Rosnay, P., Balsamo, G., Andersson, E., Bougeault, P., and Viterbo, P.: Towards a Kalman Filter based soil moisture analysis system for the operational ECMWF Integrated Forecast System, Geophysical Research Letters, 36, https://doi.org/10.1029/2009GL037716, l10401, 2009.

Dubovik, O., Holben, B., Eck, T. F., Smirnov, A., Kaufman, Y. J., King, M. D., Tanré, D., and Slutsker, I.: Variability of absorption and optical properties of key aerosol types observed in worldwide locations, Journal of the atmospheric sciences, 59, 590–608, 2002.

Dutra, E., Diamantakis, M., Tsonevsky, I., Zsoter, E., Wetterhall, F., Stockdale, T., Richardson, D., and Pappenberger, F.: The extreme forecast index at the seasonal scale, Atmospheric Science Letters, 14, 256–262, https://doi.org/10.1002/asl2.448, 2013.

EDGAR: Emission Database for Global Atmospheric Research (EDGAR), release EDGARv4.2 FT2010, Tech. rep., European Commission, Joint Research Centre (JRC)/Netherlands Environmental Assessment Agency (PBL), 2013.

Emeis, S., Forkel, R., Junkermann, W., Schäfer, K., Flentje, H., Gilge, S., Fricke, W., Wiegner, M., Freudenthaler, V., Groß, S., Ries, L., Meinhardt, F., Birmili, W., Münkel, C., Obleitner, F., and Suppan, P.: Measurement and simulation of the 16/17 April 2010 Eyjafjallajökull volcanic ash layer dispersion in the northern Alpine region, Atmospheric Chemistry and Physics, 11, 2689–2701, https://doi.org/10.5194/acp-11-2689-2011, 2011.

Engelstaedter, S. and Washington, R.: Temporal controls on global dust emissions: The role of surface gustiness, Geophysical Research Letters, 34, https://doi.org/10.1029/2007GL029971, l15805, 2007.

Fast, J. D., Gustafson, W. I., Easter, R. C., Zaveri, R. A., Barnard, J. C., Chapman, E. G., Grell, G. A., and Peckham, S. E.: Evolution of ozone, particulates, and aerosol direct radiative forcing in the vicinity of Houston using a fully coupled meteorology-chemistry-aerosol model, Journal of Geophysical Research: Atmospheres, 111, https://doi.org/10.1029/2005JD006721, 2006.

Fernald, F. G.: Analysis of atmospheric lidar observations: some comments, Appl. Opt., 23, 652–653, https://doi.org/10.1364/AO.23.000652, 1984.

Flentje, H., Claude, H., Elste, T., Gilge, S., Köhler, U., Plass-Dülmer, C., Steinbrecht, W., Thomas, W., Werner, A., and Fricke, W.: The Eyjafjallajökull eruption in April 2010 - detection of volcanic plume using in-situ measurements, ozone sondes and lidar-ceilometer profiles, Atmospheric Chemistry and Physics, 10, 10 085–10 092, https://doi.org/10.5194/acp-10-10085-2010, 2010.

Flentje, H., Briel, B., Beck, C., Coen, M. C., Fricke, M., Cyrys, J., Gu, J., Pitz, M., and Thomas, W.: Identification and monitoring of Saharan dust: An inventory representative for south Germany since 1997, Atmospheric Environment, 109, 87 – 96, https://doi.org/https://doi.org/10.1016/j.atmosenv.2015.02.023, 2015.

Forkel, R., Balzarini, A., Baró, R., Bianconi, R., Curci, G., Jiménez-Guerrero, P., Hirtl, M., Honzak, L., Lorenz, C., Im, U., Pérez, J. L., Pirovano, G., José, R. S., Tuccella, P., Werhahn, J., and Žabkar, R.: Analysis of the WRF-Chem contributions to AQMEII phase2 with respect to aerosol radiative feedbacks on meteorology and pollutant distributions, Atmospheric Environment, 115, 630 – 645, https://doi.org/https://doi.org/10.1016/j.atmosenv.2014.10.056, 2015.

Geisinger, A., Behrendt, A., Wulfmeyer, V., Strohbach, J., Förstner, J., and Potthast, R.: Development and application of a backscatter lidar forward operator for quantitative validation of aerosol dispersion models and future data assimilation, Atmospheric Measurement Techniques, 10, 4705–4726, https://doi.org/10.5194/amt-10-4705-2017, 2017.

Grell, G. A., Peckham, S. E., Schmitz, R., McKeen, S. A., Frost, G., Skamarock, W. C., and Eder, B.: Fully coupled "online" chemistry within the WRF model, Atmospheric Environment, 39, 6957 – 6975, https://doi.org/https://doi.org/10.1016/j.atmosenv.2005.04.027, 2005.

Groß, S., Freudenthaler, V., Schepanski, K., Toledano, C., Schäfler, A., Ansmann, A., and Weinzierl, B.: Optical properties of long-range transported Saharan dust over Barbados as measured by dual-wavelength depolarization Raman lidar measurements, Atmospheric Chemistry and Physics, 15, 11 067–11 080, https://doi.org/10.5194/acp-15-11067-2015, 2015.

Guelle, W., Balkanski, Y. J., Schulz, M., Marticorena, B., Bergametti, G., Moulin, C., Arimoto, R., and Perry, K. D.: Modeling the atmospheric distribution of mineral aerosol: Comparison with ground measurements and satellite observations for yearly and synoptic timescales over the North Atlantic, Journal of Geophysical Research: Atmospheres, 105, 1997–2012, https://doi.org/10.1029/1999JD901084, 2000.

Hess, M., Koepke, P., and Schult, I.: Optical properties of aerosols and clouds: The software package OPAC, Bulletin of the American meteorological society, 79, 8–844, 1998.

Im, U., Bianconi, R., Solazzo, E., Kioutsioukis, I., Badia, A., Balzarini, A., Baró, R., Bellasio, R., Brunner, D., Chemel, C., Curci, G., van der Gon, H. D., Flemming, J., Forkel, R., Giordano, L., Jiménez-Guerrero, P., Hirtl, M., Hodzic, A., Honzak, L., Jorba, O., Knote, C., Makar, P. A., Manders-Groot, A., Neal, L., Pérez, J. L., Pirovano, G., Pouliot, G., Jose, R. S., Savage, N., Schroder, W., Sokhi, R. S., Syrakov, D., Torian, A., Tuccella, P., Wang, K., Werhahn, J., Wolke, R., Zabkar, R., Zhang, Y., Zhang, J., Hogrefe, C., and Galmarini, S.: Evaluation of operational online-coupled regional air quality models over Europe and North America in the context of AQMEII phase 2. Part II: Particulate matter, Atmospheric Environment, 115, 421 – 441, https://doi.org/https://doi.org/10.1016/j.atmosenv.2014.08.072, 2015.

IPCC: IPCC, 2012: Managing the Risks of Extreme Events and Disasters to Advance Climate Change Adaptation. A Special Report of Working Groups I and II of the Intergovernmental Panel on Climate Change, Cambridge University Press, Cambridge, UK, and New York, NY, USA, 2012.

Jones, A., Roberts, D. L., Woodage, M. J., and Johnson, C. E.: Indirect sulphate aerosol forcing in a climate model with an interactive sulphur cycle, Journal of Geophysical Research: Atmospheres, 106, 20 293–20 310, https://doi.org/10.1029/2000JD000089, 2001.

Kalnay, E., Kanamitsu, M., Kistler, R., Collins, W., Deaven, D., Gandin, L., Iredell, M., Saha, S., White, G., Woollen, J., et al.: The NCEP/NCAR 40-year reanalysis project, Bulletin of the American meteorological Society, 77, 437–471, 1996.

Kandler, K., Schütz, L., Deutscher, C., Ebert, M., Hofmann, H., Jäckel, S., Jaenicke, R., Knippertz, P., Lieke, K., Massling, A., Petzold, A., Schladitz, A., Weinzierl, B., Wiedensohler, A., Zorn, S., and Weinbruch, S.: Size distribution, mass concentration, chemical and mineralogical composition and derived optical parameters of the boundary layer aerosol at Tinfou, Morocco, during SAMUM 2006, Tellus B, 61, 32–50, https://doi.org/10.1111/j.1600-0889.2008.00385.x, 2009.

Kazil, J., Stier, P., Zhang, K., Quaas, J., Kinne, S., O'Donnell, D., Rast, S., Esch, M., Ferrachat, S., Lohmann, U., and Feichter, J.: Aerosol nucleation and its role for clouds and Earth's radiative forcing in the aerosol-climate model ECHAM5-HAM, Atmospheric Chemistry and Physics, 10, 10 733–10 752, https://doi.org/10.5194/acp-10-10733-2010, 2010.

Klett, J. D.: Stable analytical inversion solution for processing lidar returns, Appl. Opt., 20, 211–220, https://doi.org/10.1364/AO.20.000211, 1981.

Köpke, P., Hess, M., Schult, I., and Shettle, E.: Global aerosol data set, Max-Planck-Institut für Meteorologie Hamburg, Germany, 1997.

Lohmann, U., Stier, P., Hoose, C., Ferrachat, S., Kloster, S., Roeckner, E., and Zhang, J.: Cloud microphysics and aerosol indirect effects in the global climate model ECHAM5-HAM, Atmospheric Chemistry and Physics, 7, 3425–3446, https://doi.org/10.5194/acp-7-3425-2007, 2007.

Madonna, F., Amato, F., Vande Hey, J., and Pappalardo, G.: Ceilometer aerosol profiling versus Raman lidar in the frame of the INTERACT campaign of ACTRIS, Atmospheric Measurement Techniques, 8, 2207–2223, https://doi.org/10.5194/amt-8-2207-2015, 2015.

Mann, G. W., Carslaw, K. S., Ridley, D. A., Spracklen, D. V., Pringle, K. J., Merikanto, J., Korhonen, H., Schwarz, J. P., Lee, L. A., Manktelow, P. T., Woodhouse, M. T., Schmidt, A., Breider, T. J., Emmerson, K. M., Reddington, C. L., Chipperfield, M. P., and Pickering, S. J.: Intercomparison of modal and sectional aerosol microphysics representations within the same 3-D global chemical transport model, Atmospheric Chemistry and Physics, 12, 4449–4476, https://doi.org/10.5194/acp-12-4449-2012, 2012.

Mishchenko, M. I. and Travis, L. D.: Capabilities and limitations of a current FORTRAN implementation of the T-matrix method for randomly oriented, rotationally symmetric scatterers, Journal of Quantitative Spectroscopy and Radiative Transfer, 60, 309–324, https://doi.org/https://doi.org/10.1016/S0022-4073(98)00008-9, 1998.

Mishchenko, M. I., Dlugach, J. M., Yanovitskij, E. G., and Zakharova, N. T.: Bidirectional reflectance of flat, optically thick particulate layers: an efficient radiative transfer solution and applications to snow and soil surfaces, Journal of Quantitative Spectroscopy and Radiative Transfer, 63, 409–432, https://doi.org/http://dx.doi.org/10.1016/S0022-4073(99)00028-X, 1999.

Mona, L., Papagiannopoulos, N., Basart, S., Baldasano, J., Binietoglou, I., Cornacchia, C., and Pappalardo, G.: EARLINET dust observations vs. BSC-DREAM8b modeled profiles: 12-year-long systematic comparison at Potenza, Italy, Atmospheric Chemistry and Physics, 14, 8781–8793, https://doi.org/10.5194/acp-14-8781-2014, 2014.

Morcrette, J.-J., Beljaars, A., Benedetti, A., Jones, L., and Boucher, O.: Sea-salt and dust aerosols in the ECMWF IFS model, Geophysical Research Letters, 35, https://doi.org/10.1029/2008GL036041, l24813, 2008.

Morcrette, J.-J., Boucher, O., Jones, L., Salmond, D., Bechtold, P., Beljaars, A., Benedetti, A., Bonet, A., Kaiser, J. W., Razinger, M., Schulz, M., Serrar, S., Simmons, A. J., Sofiev, M., Suttie, M., Tompkins, A. M., and Untch, A.: Aerosol analysis and forecast in the European Centre for Medium-Range Weather Forecasts Integrated Forecast System: Forward modeling, Journal of Geophysical Research: Atmospheres, 114, https://doi.org/10.1029/2008JD011235, d06206, 2009.

Müller, D., Heinold, B., Tesche, M., Tegen, I., Althausen, D., Arboledas, L. A., Amiridis, V., Amodeo, A., Ansmann, A., Balis, D., Comeron, A., D'amico, G., Gerasopoulos, E., Guerrero-Rascado, J. L., Freudenthaler, V., Giannakaki, E., Heese, B., Iarlori, M., Knippertz, P., Mamouri, R. E., Mona, L., Papayannis, A., Pappalardo, G., Perrone, R.-M., Pisani, G., Rizi, V., Sicard, M., Spinelli, N., Tafuro, A., and Wiegner, M.: EARLINET observations of the 14-22 May long-range dust transport event during SAMUM 2006: validation of results from dust transport modelling, Tellus B, 61, 325–339, https://doi.org/10.1111/j.1600-0889.2008.00400.x, 2009.

O'Dowd, C. D., Lowe, J. A., Smith, M. H., Davison, B., Hewitt, C. N., and Harrison, R. M.: Biogenic sulphur emissions and inferred non-sea-salt-sulphate cloud condensation nuclei in and around Antarctica, Journal of Geophysical Research: Atmospheres, 102, 12 839–12 854, https://doi.org/10.1029/96JD02749, 1997.

Rabier, F., Jarvinen, H., Klinker, E., Mahfouf, J.-F., and Simmons, A.: The ECMWF operational implementation of four-dimensional variational assimilation. I: Experimental results with simplified physics, Quarterly Journal of the Royal Meteorological Society, 126, 1143–1170, https://doi.org/10.1002/qj.49712656415, 2000.

Rao, S. T., Galmarini, S., and Puckett, K.: Air Quality Model Evaluation International Initiative (AQMEII): Advancing the State of the Science in Regional Photochemical Modeling and Its Applications, Bulletin of the American Meteorological Society, 92, 23–30, https://doi.org/10.1175/2010BAMS3069.1, 2011.

Reddy, M. S., Boucher, O., Bellouin, N., Schulz, M., Balkanski, Y., Dufresne, J.-L., and Pham, M.: Estimates of global multicomponent aerosol optical depth and direct radiative perturbation in the Laboratoire de Meteorologie Dynamique general circulation model, Journal of Geophysical Research: Atmospheres, 110, https://doi.org/10.1029/2004JD004757, d10S16, 2005.

Shettle, E. P. and Fenn, R. W.: Models for the aerosols of the lower atmosphere and the effects of humidity variations on their optical properties, Tech. Rep. Environmental research papers No. 675, NTIS, ADA 085951, AFGL-TR-79-0214, Air Force Geophysics Lab Hanscom Afb Ma, 1979.

Siomos, N., Balis, D. S., Poupkou, A., Liora, N., Dimopoulos, S., Melas, D., Giannakaki, E., Filioglou, M., Basart, S., and Chaikovsky, A.: Investigating the quality of modeled aerosol profiles based on combined lidar and sunphotometer data, Atmospheric Chemistry and Physics, 17, 7003–7023, https://doi.org/10.5194/acp-17-7003-2017, 2017.

Solazzo, E., Bianconi, R., Pirovano, G., Matthias, V., Vautard, R., Moran, M. D., Appel, K. W., Bessagnet, B., Brandt, J., Christensen, J. H., Chemel, C., Coll, I., Ferreira, J., Forkel, R., Francis, X. V., Grell, G., Grossi, P., Hansen, A. B., Miranda, A. I., Nopmongcol, U., Prank, M., Sartelet, K. N., Schaap, M., Silver, J. D., Sokhi, R. S., Vira, J., Werhahn, J., Wolke, R., Yarwood, G., Zhang, J., Rao, S. T., and Galmarini, S.: Operational model evaluation for particulate matter in Europe and North America in the context of AQMEII, Atmospheric Environment, 53, 75 – 92, https://doi.org/https://doi.org/10.1016/j.atmosenv.2012.02.045, 2012.

Stier, P., Feichter, J., Kinne, S., Kloster, S., Vignati, E., Wilson, J., Ganzeveld, L., Tegen, I., Werner, M., Balkanski, Y., Schulz, M., Boucher, O., Minikin, A., and Petzold, A.: The aerosol-climate model ECHAM5-HAM, Atmospheric Chemistry and Physics, 5, 1125–0156, https://doi.org/10.5194/acp-5-1125-2005, 2005.

Stuut, J.-B., Smalley, I., and O'Hara-Dhand, K.: Aeolian dust in Europe: African sources and European deposits, Quaternary International, 198, 234–245, https://doi.org/http://dx.doi.org/10.1016/j.quaint.2008.10.007, loess in the Danube Region and Surrounding Loess Provinces: The Marsigli Memorial Volume, 2009.

Swietlicki, E., Hansson, H.-C., Hämeri, K., Svenningsson, B., Massling, A., Mcfiggans, G., Mcmurry, P. H., PetäJä, T., Tunved, P., Gysel, M., Topping, D., Weingartner, E., Baltensperger, U., Rissler, J., Wiedensohler, A., and Kulmala, M.: Hygroscopic properties of submicrometer atmospheric aerosol particles measured with H-TDMA instruments in various environments — a review, Tellus B, 60, 432–469, https://doi.org/10.1111/j.1600-0889.2008.00350.x, 2008.

van der Gon, H. D., Beevers, S., D'Allura, A., Finardi, S., Honoré, C., Kuenen, J., Perrussel, O., Radice, P., Theloke, J., Uzbasich, M., and Visschedijk, A.: Discrepancies Between Top-Down and Bottom-Up Emission Inventories of Megacities: The Causes and Relevance for Modeling Concentrations and Exposure, in: Air Pollution Modeling and its Application XXI, edited by Steyn, D. G. and Trini Castelli, S., pp. 199–204, Springer Netherlands, Dordrecht, 2012.

van der Werf, G. R., Randerson, J. T., Giglio, L., Collatz, G. J., Mu, M., Kasibhatla, P. S., Morton, D. C., DeFries, R. S., Jin, Y., and van Leeuwen, T. T.: Global fire emissions and the contribution of deforestation, savanna, forest, agricultural, and peat fires (1997-2009), Atmospheric Chemistry and Physics, 10, 11 707–11 735, https://doi.org/10.5194/acp-10-11707-2010, 2010.

Wang, M., Ghan, S., Ovchinnikov, M., Liu, X., Easter, R., Kassianov, E., Qian, Y., and Morrison, H.: Aerosol indirect effects in a multi-scale aerosol-climate model PNNL-MMF, Atmospheric Chemistry and Physics, 11, 5431–5455, https://doi.org/10.5194/acp-11-5431-2011, 2011.

Wang, Y., Sartelet, K. N., Bocquet, M., Chazette, P., Sicard, M., D'Amico, G., Léon, J. F., Alados-Arboledas, L., Amodeo, A., Augustin, P., Bach, J., Belegante, L., Binietoglou, I., Bush, X., Comerón, A., Delbarre, H., García-Vízcaino, D., Guerrero-Rascado, J. L., Hervo, M., Iarlori, M., Kokkalis, P., Lange, D., Molero, F., Montoux, N., Muñoz, A., Muñoz, C., Nicolae, D., Papayannis, A., Pappalardo, G., Preissler, J., Rizi, V., Rocadenbosch, F., Sellegri, K., Wagner, F., and Dulac, F.: Assimilation of lidar signals: application to aerosol forecasting in the western Mediterranean basin, Atmospheric Chemistry and Physics, 14, 12 031–12 053, https://doi.org/10.5194/acp-14-12031-2014, 2014.

Waterman, P. C.: Symmetry, Unitarity, and Geometry in Electromagnetic Scattering, Phys. Rev. D, 3, 825–839, https://doi.org/10.1103/PhysRevD.3.825, 1971.

Wiegner, M. and Gasteiger, J.: Correction of water vapor absorption for aerosol remote sensing with ceilometers, Atmospheric Measurement Techniques, 8, 3971–3984, https://doi.org/10.5194/amt-8-3971-2015, 2015.

Wiegner, M. and Geiß, A.: Aerosol profiling with the Jenoptik ceilometer CHM15kx, Atmospheric Measurement Techniques, 5, 1953–1964, https://doi.org/10.5194/amt-5-1953-2012, 2012.

Wiegner, M., Gasteiger, J., Kandler, K., Weinzierl, B., Rasp, K., Esselborn, M., Freudenthaler, V., Heese, B., Toledano, C., Tesche, M., and Althausen, D.: Numerical simulations of optical properties of Saharan dust aerosols with emphasis on lidar applications, Tellus B, 61, 180–194, https://doi.org/10.1111/j.1600-0889.2008.00381.x, 2009.

Wiegner, M., Groß, S., Freudenthaler, V., Schnell, F., and Gasteiger, J.: The May/June 2008 Saharan dust event over Munich: Intensive aerosol parameters from lidar measurements, Journal of Geophysical Research: Atmospheres, 116, https://doi.org/10.1029/2011JD016619, 2011.

Wiegner, M., Madonna, F., Binietoglou, I., Forkel, R., Gasteiger, J., Geiß, A., Pappalardo, G., Schäfer, K., and Thomas, W.: What is the benefit of ceilometers for aerosol remote sensing? An answer from EARLINET, Atmospheric Measurement Techniques, 7, 1979–1997, https://doi.org/10.5194/amt-7-1979-2014, 2014.

Zhang, K., O'Donnell, D., Kazil, J., Stier, P., Kinne, S., Lohmann, U., Ferrachat, S., Croft, B., Quaas, J., Wan, H., Rast, S., and Feichter, J.: The global aerosol-climate model ECHAM-HAM, version 2: sensitivity to improvements in process representations, Atmospheric Chemistry and Physics, 12, 8911–8949, https://doi.org/10.5194/acp-12-8911-2012, 2012.

Zhang, Y., Seigneur, C., Seinfeld, J. H., Jacobson, M. Z., and Binkowski, F. S.: Simulation of Aerosol Dynamics: A Comparative Review of Algorithms Used in Air Quality Models, Aerosol Science and Technology, 31, 487–514, https://doi.org/10.1080/027868299304039, 1999.

Zieger, P., Fierz-Schmidhauser, R., Weingartner, E., and Baltensperger, U.: Effects of relative humidity on aerosol light scattering: results from different European sites, Atmospheric Chemistry and Physics, 13, 10 609–10 631, https://doi.org/10.5194/acp-13-10609-2013, 2013.

Appendix A

The aerosol microphysical and optical properties at ceilometer and lidar applications relevant wavelengths are listed in Table A1. The wavelengths corresponding to Nd:YAG-lasers used for aerosol remote sensing (355 nm, 532 nm and 1064 nm), the widely used Vaisala ceilometers (910 nm), and the 'typical wavelength' for radiative transfer calculations in the shortwave spectral range (550 nm) are shown.

Table A1. Microphysical properties of dry aerosols assumed in the model.

Aerosol Type	Wavelength (λ, nm)	Density (ϱ_p, g/cm^3)	Modal Radius (r$_0$, μm)	Geometric Standard Deviation (σ_g)	Refractive Index (n)	Single Scattering Albedo (ω_0)	Specific Extinction Cross Section (σ_e^*, m^2/g)	Lidar Ratio (S_p, sr)
Sea Salt (bin 1)[a]	355	2.160	0.1002,1.0020[c]	1.9,2.0[c]	1.5156-0.0002i	1.00	6.37	56.9
Sea Salt (bin 2)[a]	355	2.160	0.1002,1.0020[c]	1.9,2.0[c]	1.5156-0.0002i	0.99	0.57	13.5
Sea Salt (bin 3)[a]	355	2.160	0.1002,1.0020[c]	1.9,2.0[c]	1.5156-0.0002i	0.97	0.16	18.8
Dust (bin 1)[b]	355	2.610	0.2900	2.0	1.4800-0.0025i	0.97	2.09	16.6
Dust (bin 2)[b]	355	2.610	0.2900	2.0	1.4800-0.0025i	0.94	0.99	19.2
Dust (bin 3)[b]	355	2.610	0.2900	2.0	1.4800-0.0025i	0.89	0.40	29.5
Organic Matter	355	1.769	0.0355	2.0	1.5280-0.0000i	1.00	5.69	35.5
Black Carbon	355	1.000	0.0118	2.0	1.7500-0.4500i	0.29	16.47	96.9
Sulfate	355	1.769	0.0355	2.0	1.5280-0.0000i	1.00	5.69	35.5
Sea Salt (bin 1)[a]	532	2.160	0.1002,1.0020[c]	1.9,2.0[c]	1.5156-0.0002i	1.00	3.56	76.0
Sea Salt (bin 2)[a]	532	2.160	0.1002,1.0020[c]	1.9,2.0[c]	1.5156-0.0002i	0.99	0.61	14.5
Sea Salt (bin 3)[a]	532	2.160	0.1002,1.0020[c]	1.9,2.0[c]	1.5156-0.0002i	0.98	0.17	15.7
Dust (bin 1)[b]	532	2.610	0.2900	2.0	1.4800-0.0018i	0.99	2.61	38.1
Dust (bin 2)[b]	532	2.610	0.2900	2.0	1.4800-0.0018i	0.96	0.88	9.5
Dust (bin 3)[b]	532	2.610	0.2900	2.0	1.4800-0.0018i	0.94	0.42	23.0
Organic Matter	532	1.769	0.0355	2.0	1.5227-0.0000i	1.00	3.25	42.3
Black Carbon	532	1.000	0.0118	2.0	1.7500-0.4500i	0.21	9.84	98.7
Sulfate	532	1.769	0.0355	2.0	1.5227-0.0000i	1.00	3.25	42.3
Sea Salt (bin 1)[a]	550	2.160	0.1002,1.0020[c]	1.9,2.0[c]	1.5156-0.0002i	1.00	3.33	74.0
Sea Salt (bin 2)[a]	550	2.160	0.1002,1.0020[c]	1.9,2.0[c]	1.5156-0.0002i	0.99	0.61	14.6
Sea Salt (bin 3)[a]	550	2.160	0.1002,1.0020[c]	1.9,2.0[c]	1.5156-0.0002i	0.98	0.17	15.4
Dust (bin 1)[b]	550	2.610	0.2900	2.0	1.4800-0.0016i	0.99	2.63	40.9
Dust (bin 2)[b]	550	2.610	0.2900	2.0	1.4800-0.0016i	0.97	0.87	9.9
Dust (bin 3)[b]	550	2.610	0.2900	2.0	1.4800-0.0016i	0.94	0.43	20.4
Organic Matter	550	1.769	0.0355	2.0	1.5220-0.0000i	1.00	3.07	42.5
Black Carbon	550	1.000	0.0118	2.0	1.7500-0.4500i	0.21	9.41	99.8
Sulfate	550	1.769	0.0355	2.0	1.5220-0.0000i	1.00	3.07	42.5
Sea Salt (bin 1)[a]	910	2.160	0.1002,1.0020[c]	1.9,2.0[c]	1.5156-0.0002i	1.00	0.89	36.0
Sea Salt (bin 2)[a]	910	2.160	0.1002,1.0020[c]	1.9,2.0[c]	1.5156-0.0002i	1.00	0.63	11.6
Sea Salt (bin 3)[a]	910	2.160	0.1002,1.0020[c]	1.9,2.0[c]	1.5156-0.0002i	0.99	0.17	15.9
Dust (bin 1)[b]	910	2.610	0.2900	2.0	1.4800-0.0006i	1.00	1.91	74.5
Dust (bin 2)[b]	910	2.610	0.2900	2.0	1.4800-0.0006i	1.00	1.54	35.2
Dust (bin 3)[b]	910	2.610	0.2900	2.0	1.4800-0.0006i	0.98	0.41	11.8
Organic Matter	910	1.769	0.0355	2.0	1.5114-0.0000i	1.00	1.12	37.5
Black Carbon	910	1.000	0.0118	2.0	1.7500-0.4500i	0.11	4.78	140.3
Sulfate	910	1.769	0.0355	2.0	1.5114-0.0000i	1.00	1.12	37.5
Sea Salt (bin 1)[a]	1064	2.160	0.1002,1.0020[c]	1.9,2.0[c]	1.5156-0.0002i	1.00	0.55	21.7
Sea Salt (bin 2)[a]	1064	2.160	0.1002,1.0020[c]	1.9,2.0[c]	1.5156-0.0002i	1.00	0.62	10.0
Sea Salt (bin 3)[a]	1064	2.160	0.1002,1.0020[c]	1.9,2.0[c]	1.5156-0.0002i	0.99	0.18	18.2
Dust (bin 1)[b]	1064	2.610	0.2900	2.0	1.4800-0.0006i	1.00	1.50	78.6
Dust (bin 2)[b]	1064	2.610	0.2900	2.0	1.4800-0.0006i	1.00	1.61	48.6
Dust (bin 3)[b]	1064	2.610	0.2900	2.0	1.4800-0.0006i	0.99	0.44	13.4
Organic Matter	1064	1.769	0.0355	2.0	1.5068-0.0000i	1.00	0.77	34.2
Black Carbon	1064	1.000	0.0118	2.0	1.7500-0.4500i	0.08	3.90	168.3
Sulfate	1064	1.769	0.0355	2.0	1.5068-0.0000i	1.00	0.77	34.2

[a] Sea salt aerosols are represented in the model by three size bins with the bin limits set to 0.015-0.251 μm (bin 1), 0.251-2.515 μm (bin 2) and 2.515-10.060 μm (bin 3).
[b] Dust aerosols are represented in the model by three size bins with the bin limits are set to 0.03-0.55 μm (bin 1), 0.55-0.90 μm (bin 2) and 0.90-20.00 μm (bin 3).
[c] A bimodal lognormal size distribution is assumed for sea salt aerosols, with r$_0$=0.1002 μm and 1.002 μm and σ_g=1.9 and 2.0. The number concentrations N_1 and N_2 of the first and second mode are 70 and 3 cm^{-1}, respectively.
Note that density of hydrophilic aerosol changes with hygroscopic growth of particle.

Fig. A1a shows the time-height cross section of the attenuated backscatter of the ceilometer at Alfeld, $\sim$250 km south of Elpersbüttel, on 2 April 2016 and in Fig. A1b the corresponding profiles calculated from the model output (blue curve) and retrieved from the ceilometer (red curve). Dust particles are treated as nonspherical particles as defined in Section 4.1.2. Note, that due to cloud filtering some ceilometer profiles stopped at a relatively low altitude. Similar plots for 3 and 4 April 2016 are shown in Fig. A2 and Fig. A3.

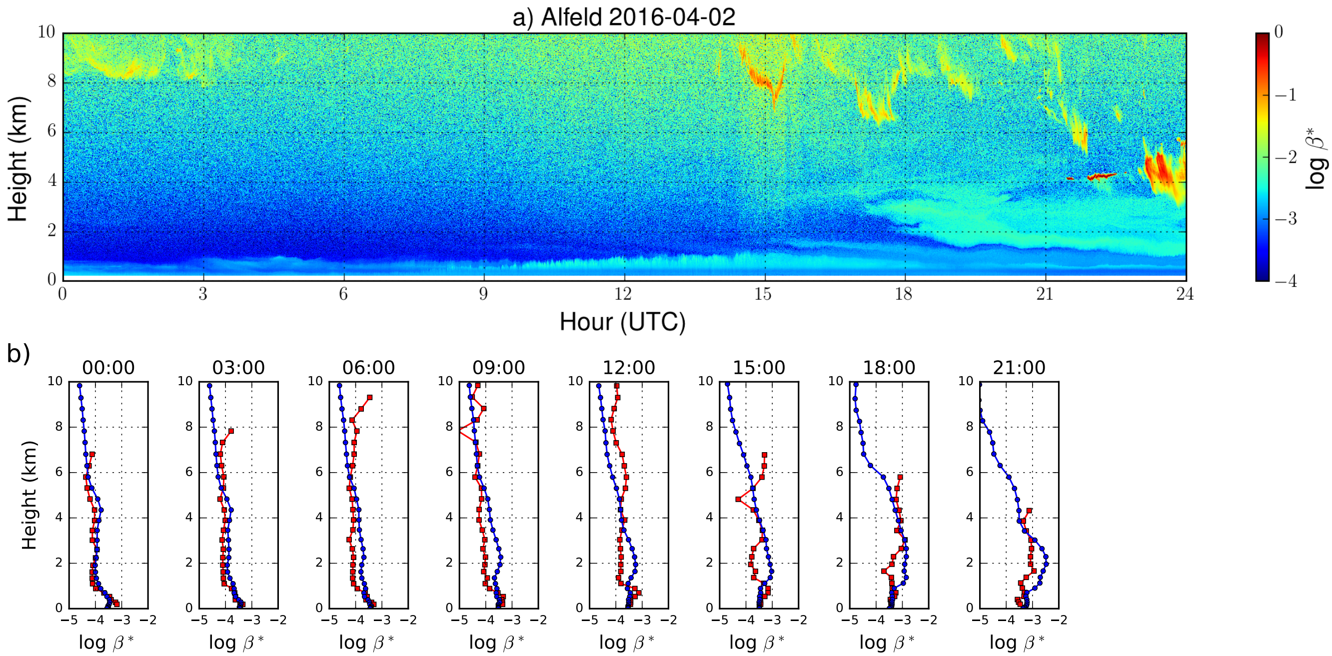

Figure A1. Time series of attenuated backscatter measured by the ceilometer (upper panel) and simulated by the model (lower panel) at Alfeld during a dust episode on 2 April 2016.

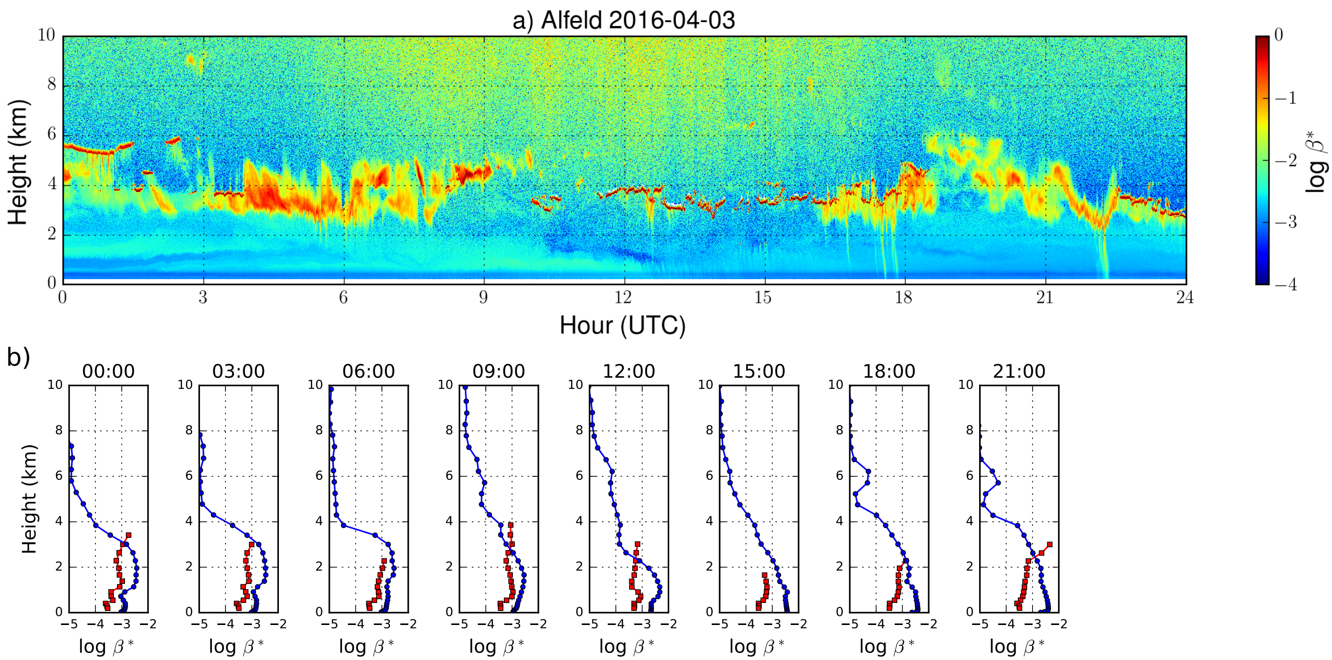

Figure A2. Time series of attenuated backscatter measured by the ceilometer (upper panel) and simulated by the model (lower panel) at Alfeld during a dust episode on 3 April 2016.

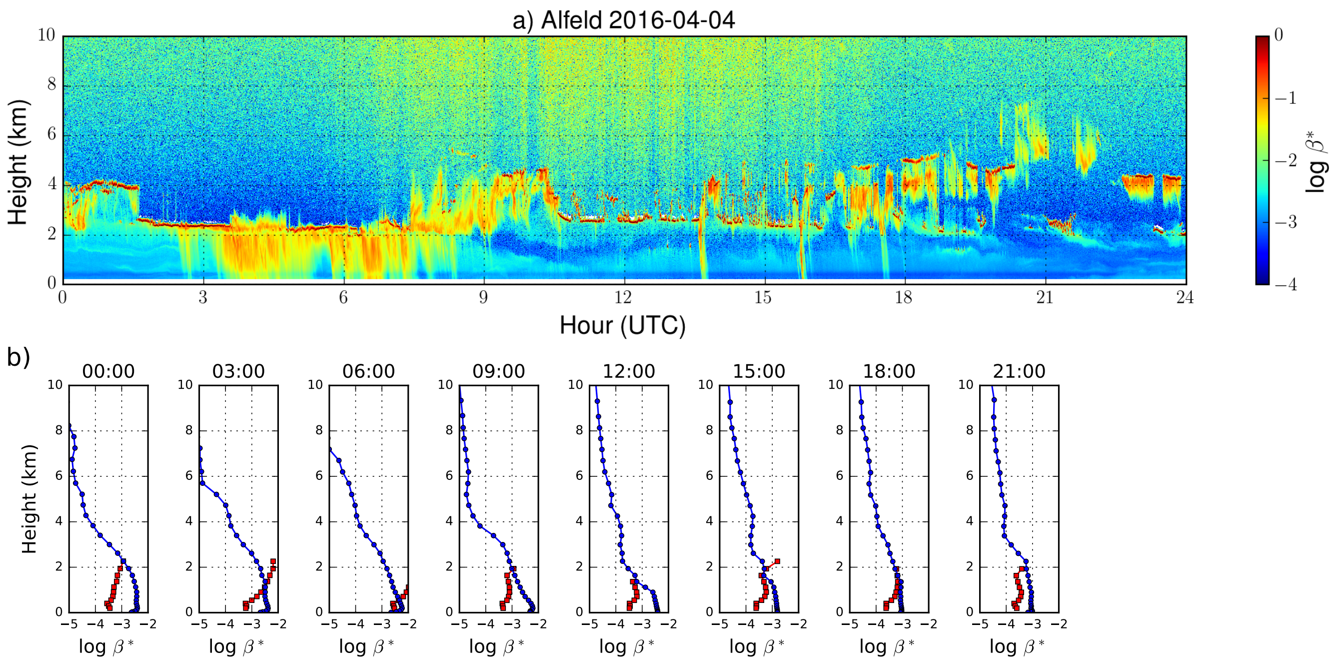

Figure A3. Time series of attenuated backscatter measured by the ceilometer (upper panel) and simulated by the model (lower panel) at Alfeld during a dust episode on 4 April 2016.